DENSITY-FUNCTIONAL THEORY APPLIED TO PROBLEMS IN CATALYSIS AND ELECTROCHEMISTRY

by

SANTOSH KUMAR
B. Tech. (Hons.) Indian Institute of Technology
Kharagpur, India 2004

A thesis submitted in partial fulfillment of the requirements
for the degree of Master of Science
in the Department of Mechanical, Materials and Aerospace Engineering
in the College of Engineering and Computer Science
at the University of Central Florida
Orlando, Florida

Summer Term
2006

ABSTRACT

We study the structure and energetics of water molecules adsorbed at ceria (111) surfaces below one monolayer coverage using density-functional theory. The results of this study provide a theoretical framework for interpreting recent experimental results on the redox properties of water at ceria (111) surfaces. In particular, we have computed the structure and energetics of various absorption geometries at stoichiometric ceria (111) surface. In contrast to experiment results, we do not find a strong coverage dependence of the adsorption energy. For the case of reduced surface, our results show that it may not be energetically favorable for water to oxidize oxygen vacancy site at the surface. Instead, oxygen vacancies tend to result in water more strongly binding to the surface. The result of this attractive water-vacancy interaction is that the apparent concentration of oxygen vacancies at the surface is enhanced in the presence of water. Finally, we discuss this problem with reference to recent experimental and theoretical studies of vacancy clustering at the (111) ceria surface.

We also describe the simulation results for the structure and dynamics of liquid water using the SIESTA electronic structure approach. We find that the structure of water depends strongly on the particular basis set used. Applying a systematic approach to varying the basis set, we find that the basis set which results in good agreement with experimental binding energies for isolated water dimers also provides a reasonable description of the radial distribution functions of liquid water. We show that the structure of liquid water varies in a systematic fashion with the choice of basis set. Comparable to many other first-principle studies of liquid water using gradient-corrected density functionals, the liquid is found to be somewhat overstructured. The possibility of further improvements through a better choice of the basis set is discussed. We find

that while improvements are likely to be possible, application to large-scale systems will require use of a computational algorithm whose computational cost scales linearly with system size.

Finally, we study the molecular and atomic adsorption of oxygen on the gold nano-clusters. We show multiple stable and metastable structures for atomically and molecularly adsorbed oxygen to the gold cluster. We plan to predict the reaction pathway and calculate activation energy barrier for desorption of molecular oxygen from the atomically adsorbed gold cluster which is very important for any catalytic reaction occurring using gold nanoparticles.

ACKNOWLEDGMENTS

I take this opportunity to thank Dr. Patrick K. Schelling, my advisor, for his constant help, advice and guidance on this research and with this thesis.

TABLE OF CONTENTS

LIST OF FIGURES

LIST OF TABLES

LIST OF ACRONYMS

DFT	Density Functional Theory
VASP	Vienna Ab Initio Simulation Package
SIESTA	Spanish Initiative for Electronic Simulations with Thousands of Atoms
MD	Molecular Dynamics
SCTB	Self-Consistent Tight-Binding
LDA	Local Density Approximation
GGA	Generalized Gradient Approximation
PAW	Projector Augmented Wave
LCAO	Linear Combination of Atomic Orbitals
PAO	pseudo-atomic orbitals
TWC	Three Way Catalysis
OSC	Oxygen Storage Capacity
TPD	Temperature Programmed Desorption
MEP	Minimum Energy Path
WGS	Water Gas Shift

CHAPTER 1 : INTRODUCTION

Air pollution is one of the major global problems threatening modern civilization. It makes environmental friendly technologies to be a requirement of today and catalysis has become an important tool to drive the growth of such technologies in recent years. Catalysis science investigates the dynamics of the elementary surface reaction steps on the atomic scale and the relationship of the atomic surface structure and surface composition to the catalytic process. Rare-earth oxides have been widely investigated as structural and electronic promoters to improve the activity, selectivity and thermal stability of catalysts. The most significant of the oxides of rare-earth elements in industrial catalysis is certainly CeO_2. Its use in catalysis has attracted considerable attention in recent years, especially for those applications, such as treatment of emissions, where ceria has shown great potential [1]. This is documented well by the increasing number of scientific articles and patents that have appeared on this topic in the last few years.

There are also several emerging applications on process for which cerium oxide is currently being actively investigated. Specifically, CeO_2 has potential uses for removal of soot from diesel engine exhaust [2], for the removal of organics from wastewaters (catalytic wet oxidation) [3], as an additive for combustion catalysts and processes [4], and in redox and electrochemical reactions. In addition to these applications, much effort has been dedicated recently to studying the role of ceria in well-established industrial processes such as Fluid Catalytic Cracking and Three-way-Catalysts (TWC), where CeO_2 is a key component in catalyst formulation. TWC is also very widely used for gasoline-fuelled engine exhaust gas treatment.

TWC must simultaneously reduce NO_x and oxidize CO and hydrocarbons. An optimum conversion of these pollutants is only obtained around the stoichiometry. However, under real driving conditions, exhaust gas composition vary drastically. So to maintain constant overall efficiency of TWC support materials is required to store oxygen under lean conditions and to release oxygen under fuel rich conditions. This particular property of storing and releasing oxygen is called Oxygen Storage Capacity (OSC) and ceria fits into this role very well as it has the ability to store, release, and transport oxygen ions. Application of OSC of ceria exploit the amazing property of the cerium (IV) oxide to release oxygen under reduction conditions forming a series of reduced oxides with stoichiometric cerium (III) oxide as an end product, which in its turn easily takes up oxygen under oxidizing conditions, turning the (III) oxide back into ceria. In other words this oxygen storage capacity of ceria is closely related to the formation and migration of oxygen vacancies or its ability to shift oxidation states [5].

Many other critical catalytic reactions depend on the behavior of water at oxide surfaces. For example, in many catalyst applications, water is often present either as reactant or as spectator. Electrochemical reactions often occur at the interface between water and an oxide passive layer. To begin to understand the complex behavior of these systems, it is essential to develop an atomic-scale description of structure and dynamics.

In recent years, atomic-scale simulation has been increasingly been used to fill this important need. One of the earliest applications of density-functional theory (DFT) to water-oxide interfaces was to study water dissociation at the rutile (110) surface [6]. Since this groundbreaking study, the role of simulation has gained increasing acceptance as a useful tool in elucidating the properties of the water-oxide interface. In addition to many important DFT studies, there have also been inventive and useful applications of classical molecular-dynamics

(MD) simulations. More recently, there has been an effort to apply self-consistent tight-binding (SCTB) models to this area, with the important goal of treating systems on a longer length and time scale than traditional DFT approaches [7]. In summary, the application of atomic-scale simulation studies of the oxide-water interface is an important tool for understanding the properties of water-oxide interfaces.

Motivation and overview

As discussed earlier, ceria is one of an important oxide for support of metallic-catalyst nanoparticles. One especially important function of ceria is in the water-gas shift (WGS) reaction, described by

$$CO + H_2O \rightarrow CO_2 + H_2 \qquad (1.1)$$

Recently, experiments have shown that redox chemistry of water at ceria surfaces depends strongly on the particular surface orientation. In particular, early works appear to show that under most conditions water will tend to oxidize the reduced ceria films and powder [8-10]. In contrast to these studies, there is a report of water causing further reduction of a thin ceria film on a Pt (111) substrate [11]. However, these studies did not offer the possibility of studying the dependence of the chemistry on the surface morphology. Recently, more carefully controlled experiments have revealed that in fact the (111) face is likely different from other low-index faces [12]. In particular, water appears to reduce rather than oxidize reduced (111) ceria surface. Experiments have shown that the vacancy concentration at the (111) surface appears to increase in the presence of water vapor. As noted by the authors of Ref. [12], this presents the interesting possibility that systems with more than one facet exposed to an environment may undergo simultaneous reduction and oxidation reactions. This important result may have significant

implications for catalyst applications. So, we decided to take up a theoretical study of the behavior of water at the ceria (111) surface using DFT.

But before we take up the atomic-level simulation study of water on any oxides we needed to develop a better understanding of the properties of water and its interactions with other materials as it is an important component of a wide range of research areas, including catalysis, for example, electrochemistry, biology and geology. The structure and properties of liquid water are quite subtle, and theoretical modeling has been ongoing challenge. The challenge is understood to originate from the unique nature of the hydrogen-bonded network in the liquid water. Because the structure of liquid water depends in a sensitive way on the properties of hydrogen bonds which tend to be rather weak (~0.2 eV) compared to most other chemical bonds, even very small errors tend to result in unrealistic behavior. First-principles simulation is an attractive approach that can simultaneously bring accuracy and flexibility to the problem. However, while accuracy and flexibility is critical components in any model, the computational cost associated with first-principles approach prevents their application to problems that involve large length and time scales. As a result, computational efficiency is a consideration of often equal importance to accuracy. One way to get better computational efficiency in first-principle calculation is use an approximate O(N) algorithm which scale linearly with system size and could easily be used for larger systems. Here we used one such method which utilizes local basis set of atomic orbitals which is advantageous over the traditional plane wave methods in terms of computational time but it does not give a model as good as that obtained from plane wave methods. Our model of bulk water using local basis set is able to predict chemistry and structure accurately.

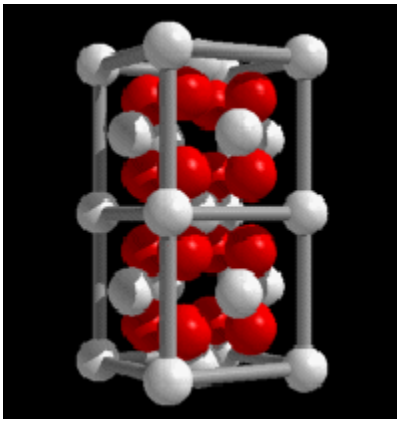

Figure 1.1: Fluorite Structure of ceria; White balls showing Ce ions at fcc position and red balls showing O ions at tetrahedral positions.

Organization of this thesis

This thesis has been divided into four parts. In first part, we have presented a review on the atomistic simulation tools with emphasis on the methods used for this work. Then in next part, we have presented the study of water adsorption at the reduced and stoichiometric ceria (111) surface. Another part of this thesis has been devoted to the study of liquid water using a novel first-principle method that employs a small basis set of atomic orbitals. Finally, a first principle study of gold cluster with molecular oxygen is presented.

CHAPTER 2 : METHODOLOGY

In this section, we are discussing the highlights of many-body problem which are relevant to the understanding of electronic structure and properties.

First Principles Calculations

Ab initio methods are distinguished from empirical methods by requiring only atomic number as input. Energy, structure, and other properties of a substance are calculated from these inputs strictly through the application of quantum mechanics, without recourse to any adjustable fitting parameters. *Ab initio* calculations are useful as a complement to laboratory experiments because they allow the characteristics of a modeled system to be much more closely and precisely measured than is possible in real chemical system. Far greater ability to control and manipulate a system is also offered by *ab initio* calculation compared with experiments. However the value of such details and control is of course contingent upon how accurately the model system reflects the real system. *Ab initio* methods rely upon a series of approximations in calculating the physical quantities. In light of this, the conclusions of this study based on the calculated results have been checked against experimental.

Quantum many-bodied problem

The objective of quantum ab initio calculation is to obtain the wave function **Φ** describing the desired system through the solution of Schrödinger's equation:

$$i\hbar \frac{\partial}{\partial t}\phi = H\phi \qquad (2.1)$$

The wave function Φ contains all the information available on a given system. Using separation of variables, the stationary states can be found from the time-independent Schrödinger equation:

$$H\Psi = E\Psi \qquad (2.2)$$

In the Born-Oppenheimer approximation it is assumed that the electronic degrees of freedom adjust quickly to the motion of the nuclei, and as a result it is reasonable to determine Ψ and to find the stationary states at each atomic configuration using Eq. 2.2. The evolution of the nuclear configuration is done classically with the atomic forces determined using the wave function Ψ. The Hamiltonian operator is given in terms of the electron coordinates $\mathbf{r_i}$ and nuclear coordinates $\mathbf{R_j}$ as

$$H = \sum_{i=1}^{N} \left(-1/2\nabla_i^2 + V(\mathbf{r}_i, \mathbf{R}_j) \right) + \sum_{i<j}^{N} 1/\mathbf{r}_{i,j} \qquad (2.3)$$

where N is number of electrons, $V(\mathbf{r}_i, \mathbf{R}_j) = \frac{Z_j\, e}{|\mathbf{r}_i - \mathbf{R}_j|}$ is the interaction between the electrons and nuclei, Z is charge of nuclei, e is charge of electrons and $\sum_{i<j}^{N} 1/\mathbf{r}_{i,j}$ is the electron-electron interaction.

Variational Principle

In attacking the still formidable problem of all electron equation 2.2, incorporating the Hamiltonian 2.3, use is often made of the *Rayleigh Ritz* variational method. This method takes advantage of the fact that given an arbitrary square integrable functions φ, an upper bound for the ground state energy E_o of the system governed by the Hamiltonian is provided by [13]

$$\frac{<\varphi \mid H \mid \varphi>}{<\varphi \mid \varphi>} = E[\varphi] \geq E_o \qquad (2.4)$$

How close this upper bound lies above the ground state energy value depends upon how closely the trial function φ resembles the true ground state wave function Ψ_o. In order to optimize the trial function hence minimize the upper bound, the functional E[φ] is variationally minimized i.e. φ solved for $\delta E[\varphi] = 0$.

Density functional theory

The ab initio method used in this work relies on Density Functional Theory (DFT) which has some advantages over the Hartree-Fock method. In principle, DFT is an exact account of the many-body wave function, while in practice it works on varied types of daring approximations. DFT proves the existence of a variational principle analogous to that underlying the *Rayleigh-Ritz* method except that it utilizes electron densities rather than wave functions. The electron density defined as follows:

$$\rho(\vec{\mathbf{r}}) \equiv \int \ldots \int \left|\psi(\mathbf{r}_1, \mathbf{r}_2, \ldots . \mathbf{r}_n)\right|^2 d\mathbf{r}_2 \ldots . d\mathbf{r}_n \qquad (2.5)$$

Where $\mathbf{r}_i$ is spatial coordinate of i

The sercond Hohenberg-Kohn (1964) theorem constitutes the electron density variational principle: For a trial density $\tilde{\rho}(\vec{r})$, such that $\tilde{\rho}(\vec{r}) \geq 0$ and $\int \tilde{\rho}(\vec{r}) d\vec{r} = N$ (number of electrons), $E_o \leq E\left[\tilde{\rho}(\vec{r})\right]$ where E_o is the true ground state energy and $E\left[\tilde{\rho}(\vec{r})\right]$ is the energy functional shown in equation 2.6 [14].

$$E[\rho] = T[\rho] + \int \rho(\vec{r}) V(\vec{r}) d\vec{r} + V_{ee}[\rho] \qquad (2.6)$$

$$F_{HK}[\rho] = T[\rho] + V_{ee}[\rho]$$

The only inputs into the functional $E[\rho]$ that are unique to a given system are $V(\vec{r})$, the electrostatic potential created by the nuclei, and N, the total number of electrons as a constraint on ρ. $F[\rho]$ is a universal functional in that it is independent of nuclear arrangement and charge. Unfortunately it is unknown; otherwise all electronic ground states for any nuclear configuration could be determined. DFT lays the groundwork for approaches that are more accurate than Hartee-Fock through the inclusion of correlation energy, and less complicated due to its use of the three coordinate electron density as opposed to 4N coordinate electron wavefunction. How well this potential for accuracy is realized depends upon how well $F[\rho]$ is approximated. An additional strength of DFT based methods is the fact that as better approximations to $F[\rho]$ are developed, all DFT calculations improve, regardless of systemic details, since $F[\rho]$ is universal.

Kohn-Sham method

The Kohn-Sham equations (1965) result from an attempt to circumvent the problem of the unknown $F[\rho]$ by recasting $F[\rho]$ as follows:

$$F[\rho] = T_S[\rho] + J[\rho] + E_{xc}[\rho] \tag{2.7}$$

where

$$E_{xc}[\rho] = T[\rho] - T_S[\rho] + V_{ee}[\rho] - J[\rho]$$

$T_S[\rho]$ in equation 2.7 is the kinetic energy for a system of N noninteracting electrons. $E_{xc}[\rho]$ is called exchange-correlation energy. It contains the difference in kinetic energy between a system with N interacting electrons and one with N noninteracting electrons. It also contains non-classical part of $V_{ee}[\rho]$; both the exchange part captured in Hartee-Fock theorem, and the elusive correlation energy missed by Hartee-Fock. The simplest way to approximate electon interactions is through Hartree approximation, where N- electron wavefunction is replaced by product of single-particle orbitals. By replacing $T[\rho]$ with $T_S[\rho]$, and including the difference between two kinetic energies in $E_{xc}[\rho]$, the minimization of $E[\rho]$ ultimately leads to N one-electron equations of form [15]:

$$H\varphi_i\{r\} = \left[\left(-1/2\nabla^2\right) + V_{eff}(r)\right]\varphi_i(r) = \varepsilon_i\varphi_i(r) \tag{2.8}$$

with the Kohn-Sham effective potential given by

$$V_{eff}(r) = V(r) + \frac{\delta J[\rho]}{\delta\rho(r)} + \frac{\delta E_{xc}[\rho]}{\delta\rho(r)} \tag{2.9}$$

An electron density can be derived from the N orbital solutions to equation 2.8 through the equation

$$\rho(r) = \sum_{i=1}^{N} \sum_{s} |\varphi_i(r,s)|^2 \qquad (2.10)$$

The nonlinearity of equation 2.8, due to $V_{eff}(r)$, necessitates that equation 2.8 be solved self consistently. An initial $\rho(r)$ is guessed from which $V_{eff}(r)$ is constructed by using equation 2.9. Orbitals are calculated with equation 2.8 which produce a new electron density through equation 2.10. This new electron density produces a new $V_{eff}(r)$ for the single electron equations and so on. The iterations are continued until a desired convergence in electron density ρ and associated energy $E[\rho]$ are attained.

The task of effective implementation of the Kohn-Sham method lies in finding a good approximation for E_{xc} and hence $V_{eff}(r)$. The simplest approach is the Local Density Approximation (LDA). In LDA the exchange-correlation energy of an electronic system is constructed by assuming that the exchange-correlation energy per electron at point r in the electron gas, $\varepsilon_{xc}[r]$, is equal to the exchange-correlation energy per electron in a homogeneous electron gas that has the same density as the electron gas at point r thus [15]

$$E_{xc}^{LDA}[\rho] = \int \rho(r)\varepsilon_{xc}(\rho)dr \qquad (2.11)$$

$\varepsilon_{xc}[\rho]$ equals the exchange and correlation energy per electron for uniform electron gas, which is an ordinary functional of ρ that has been parameterized from quantum Monte Carlo [13]. E_{xc}^{LDA} is a good approximation for a slowly varying electron density and becomes exact for a uniform electron gas. Surprisingly, it sometimes performs well even with rapidly varying electron densities; however with highly localized electron states it typically fails.

Purdue and Yue developed the Generalized Gradient Approximation (GGA) in an attempt to address the major source of error in LDA- the exchange energy. GGA attempts to correct for this error by incorporating polynomial terms with modulus of electron density gradient $\left(\left|\nabla\rho(r)\right|\right)$ which captures some of the deviation of the exchange-correlation energy from the uniform electron gas result.

$$E_{xc}^{GGA}[\rho] = \int_{R^3} \varepsilon_{xc}\left(\rho\uparrow(r), \rho\downarrow, \left|\nabla\rho\uparrow(r)\right|, \left|\nabla\rho\downarrow(r)\right|, ...\right)\rho(r)d^3r \qquad (2.12)$$

Like LDA, GGA has a spin polarized equivalent appropriate for use with magnetic materials. Generally GGA is more accurate than LDA in comparison with experiments. Then there is another approach called LDA+U which includes orbital dependent interactions.

The electron wave-function of Kohn-Sham orbitals can be expanded using a given basis set. These basis sets can be made from localized atomic orbitals, plane-wave or some mixed. Depending upon different basis sets many simulation packages have been developed to solve Kohn-Sham equations. For this study we used Vienna Ab Initio Simulation Package (VASP) which uses plane wave basis sets and Spanish Initiative for Electronic Simulations with Thousands of Atoms (SIESTA) which uses localized basis sets of atomic orbitals.

Vienna Ab Initio Simulation Package (VASP)

One *ab initio* simulation code used in this study was the 'Vienna Ab Initio Simulation Package" or VASP [15-18]. VASP solves the Kohn-Sham equations iteratively for valence orbitals using ultra-soft Vanderbilt pseudopotentials or alternately using potentials and the projector-augmented wave approach[19-23]. Solutions of the Kohn-Sham equations in VASP are assisted by the fact that all systems are required to have translational symmetry. This means

crystalline systems are treated appropriately by VASP, while amorphous or systems with defects are subjected to approximation of periodicity. The presence of translational symmetry means that an orbital need only be solved with in unit cell, which is assumed to repeat over infinite Bravais lattice. The imposed translational symmetry also means that Kohn-Sham orbital solutions will be Bloch functions [13, 24].

$$\varphi_i(r) = \varphi_{n.\mathbf{k}}(r) = e^{ik.r} u_{n.\mathbf{k}}(r) \tag{2.13}$$

The wave vector **k** falls in the first Brillouin zone of reciprocal space defined by the Bravais lattice and $u_{n.\mathbf{k}}(r)$ is a function with the periodicity of the bravais lattice.

In VASP, the Bloch functions or more specifically the periodic factors $u_{n.\mathbf{k}}(r)$ of the Bloch functions are expanded in plane wave basis but we should also keep in mind that VASP implements projector-augmented wave (PAW) which is a mixed basis of local states and plane wave. The momentum vectors of these plane waves are restricted to reciprocal lattice vectors due to translational symmetry of $u_{n,k}(r)$.

$$\varphi_{n,k}(r) = e^{ik.r} \sum_G c_{n,G}(k) e^{iG.r} \tag{2.14}$$

$G \equiv$ reciprocal lattice vector

If the sum is over the infinite set of reciprocal lattice vectors, then exact solutions to the K-S equations are possible. However, real world limitations require that the summation to be truncated at some point keeping in mind the tradeoff between accuracy and computational demands. VASP truncates the summation at a specified energy cutoff given by $E_{\max} = 1/2|k+G|^2$. Applying the *Rayleigh-Ritz* variational method to $\varphi_{n,k}(r)$ amounts to

$$\frac{\partial}{\partial c_{n,G}(k)} \frac{\left\langle \varphi \mid \hat{h}_{KS} \mid \varphi \right\rangle}{\left\langle \varphi \mid \varphi \right\rangle} = 0 \tag{2.15}$$

This leads to the secular determinant

$$\left| H_{KS}(k) - \varepsilon_n(k) S(k) \right| = 0 \tag{2.16}$$

$H_{KS}(k)$ is a matrix with elements of the form

$$\int e^{i(k+G).r} \hat{h}_{KS} e^{i(k+G').r} dr \tag{2.17}$$

S is a matrix with elements of the form

$$\int e^{i(k+G).r} e^{i(k+G').r} dr \tag{2.18}$$

In this manner the Kohn-Sham non-linear differential equations are transformed into matrix equations which VASP solves iteratively. As discussed earlier, the orbital solutions are subsequently turned into an electron density by equations 2.10. For numerical reasons this electron density is mixed with the electron density from the previous iteration according to Broyden/Pulay mixing scheme [25, 26] in calculating a new $V_{eff}(r)$ for new Kohn-Sham equations through equation 2.9. This loop is continued until such a time as self consistent solution for the electron density and associated energy is attained by a specific degree of convergence. Following the attainment of ground state electron density, the forces on the nuclei due to interactions between nuclei and electron density are computed and then they are moved according to some relaxation algorithm like conjugate-gradient algorithm or Molecular Dynamics (MD) in which they are moved according to Newton's second law. In other words, in order to compute a ground-state structure, the atoms are moved using a conjugate-gradient algorithm until the forces fall below some specified threshold. At each relaxation step, the

ground-state electronic structure is computed. The result of this calculation is the ground-state electronic and atomic structure. From this starting point, various physical properties can be computed, including the vibrational spectra, optical properties, energies, and reaction barriers. Alternately, one can perform an MD calculation and obtain thermodynamic averages or insight into non-equilibrium phenomena.

Spanish Initiative for Electronic Simulations with Thousands of Atoms (SIESTA)

One of the disadvantages of first-principles DFT methods like one provided by the VASP code is that practical calculations are limited to ~100 atoms and times on the order of a few picoseconds. An important and active area of research is to develop reasonably accurate methods that employ a more limited basis set. For example, several groups are exploring the use of tight-binding methods [7, 27-29]. A more far reaching objective is to employ an algorithm that takes advantage of a local basis set to result in a method that can simulate ~10^3 to ~10^4 atoms and thereby vastly increase the power and scope of electronic-structure simulations.

Instead of pursuing a tight-binding method, we used a popular package called the Spanish Initiative for Electronic Simulations with Thousands of Atoms (SIESTA) for some parts of our work. SIESTA is both a method and a computer program implementation, to perform electronic structure calculations and ab initio molecular dynamics simulations of molecules and solids. One of the SIESTA's main characteristics is that it utilizes a very general and flexible linear combination of numerical atomic orbitals (LCAO) i.e. it utilizes localized basis set of pseudo-atomic orbitals (PAOs) DFT method. While limited basis sets offer an advantage for large-scale simulation over traditional plane-wave techniques, the real promise lies in the development of

new O(N) methods with a computational cost that scales linearly with system size. So it is can be implemented for larger systems of thousands of atoms unlike VASP. One important drawback of SIESTA is a reduction in accuracy when compared to traditional ab initio methods that use, for example, a basis of plane waves.

Keeping in mind the advantages and limitations of SIESTA over other DFT methods we tried to implement it for our system of bulk water. Our objective in this work is to develop a sufficiently accurate model for bulk water so that it can be used for the simulation of larger system like chemistry of surfaces and other MD studies.

CHAPTER 3 : CERIA-WATER INTERFACE

Introduction

In this work, we apply density-functional theory calculations to elucidate the behavior of water at ceria (111) surface. In the case of stoichiometric surfaces, it is found that a single hydrogen bond with oxygen on the surface is favorable, resulting in a binding energy in good agreement with experimental temperature-programmed desorption (TPD) results. When an oxygen vacancy is added to the surface, the water molecule tends to bind more strongly to the surface. We find that, in general agreement with experiment, that the ground-state energy of absorbed water in the presence of an oxygen vacancy at the (111) surface is quite low and tends to not favor dissociation of the water and oxidation of the surface. By calculating the energetics of vacancies at the surface both in the presence and absence of a low concentration of water molecules, we are able to predict the magnitude of the enhancement of vacancy concentration at the surface due to the presence of water.

In the next section, we detail the theoretical methods, in particular DFT, applied to the study of this problem. Then next section continues to detail the results obtained for the adsorption of water molecules at ceria (111) surfaces with and without the presence of oxygen vacancies. Finally, we conclude with a discussion of the implications and directions for future theoretical and experimental inquiry.

Computational approach

In recent years DFT methods has been successfully applied to the lanthanide and actinide series compounds [30]. In particular, it has been demonstrated that a combination of existing and established techniques, including ultrasoft pseudopotentials and gradient-corrections to the exchange and correlation functional, are sufficient to describe many properties of the lanthanide compounds including CeO_2. Furthermore, increasing computing power and improved algorithms have allowed the extension of DFT methods to problems involving lanthanide which are characterized by their tightly-bound *f*-electron shell. For example, in CeO_2, the 4*f* shell on the cerium ions is tightly bound in a filled, narrow electronic band [31].

Most of the basic technical details of the calculation described in this article are identical to those used in a previous study of stoichiometric and reduced ceria surface [32]. In particular, the Kohn-Sham DFT calculations were performed using the VASP. The projector-augmented wave method [33] was implemented. The GGA functional due to Perdew *et al* [34] were used to describe the exchange and correlation interactions. The energy cutoff for the plane-wave basis set was 408 *eV* and spin-polarized calculations were performed. For the cerium atoms, the 5*s*, 5*p*, 5*d*, 4*f*, and 6*s* electrons were explicitly included as valence electrons. The oxygen atoms included 2*s* and 2*p* electrons. As described in Ref.[32], this approach yields quite good agreement with experimental measurements for the lattice parameter and bulk modulus of ceria. In particular, we find that the lattice parameter computed by VASP is 5.45 Å compared with experimental value of 5.41 Å. For the bulk modulus, we obtain a value of 194 GPa, compared with the experimental values of 204 and 236 GPa [35, 36]. The previous ceria calculations using VASP found a lattice parameter of 5.45 Å and bulk modulus of 193.5 GPa, in complete agreement with the calculations presented here.

Results

Stoichiometric (111) surface structure and energetics

Ceria is found in the cubic fluorite structure with eight oxygen neighbors for each cerium ion. The (111) surface of this structure is formed on the most dense lattice plane, and as a result can be expected to be the lowest-energy surface. From a somewhat different point-of-view, the structure of the (111) surface for the fluorite lattice breaks only one of the eight Ce-O bonds characteristic of bulk-coordinated cerium, resulting in a very low-energy surface. The structure used in our study to describe the stoichiometric (111) surface is shown in Fig 3.1. We show for clarity a few periods of the surface. However, the actual structure used in our study was comprised of only 8 cerium ions and 16 oxygen ions. To perform integration of the electronic states across Brillouin zone, we used Monkhorst-Pack grids [37] and Gaussian smearing We found that a Monkhorst-Pack mesh of 4 × 4 × 1 k-points was adequate for the convergence of the electronic structure. Using this k-point mesh resulted in a surface energy of 0.042 $eV/Å^2$. By increasing the mesh of k-points to 6 × 6 × 1 the change in surface energy of the stoichiometric surface was found to be only 0.05 %. Furthermore, the work in Ref. [32] used a 10 × 10 × 1 mesh of k-points, and found 0.037 $eV/Å^2$ for the surface energy, indicating that our much smaller mesh results in quite reasonable accuracy. There are no experimental results for the surface energy that can be used for comparison.

Table 3.1: The displacement of ions along [111] direction after relaxation for first few layer in stoichiometric ceria (111) surface.

Ion Numbers	Displacement of ions along [111] [in Å]
1	-0.01124
2	-0.01124
3	-0.00682
4	0.02710

In agreement with Ref. [32], we found that the magnitude of the surface relaxations for the stoichiometric (111) surface are very small. We show in Table 3.1 the displacements of the ions along the (111) direction for the first few layers. The ion numbers in Table 3.1 correspond to the labels in Fig. 3.1. The very small displacements are consistent with the fact that, as several different studies has shown, the (111) surface is the most stable of the low-index surfaces [38, 39]. The effect of ionic relaxation on the surface energy is very small. In particular, we find that ionic relaxation lowers the surface energy by less than 10^{-3} $eV/\text{Å}^2$, in good agreement with the results of Ref. [32].

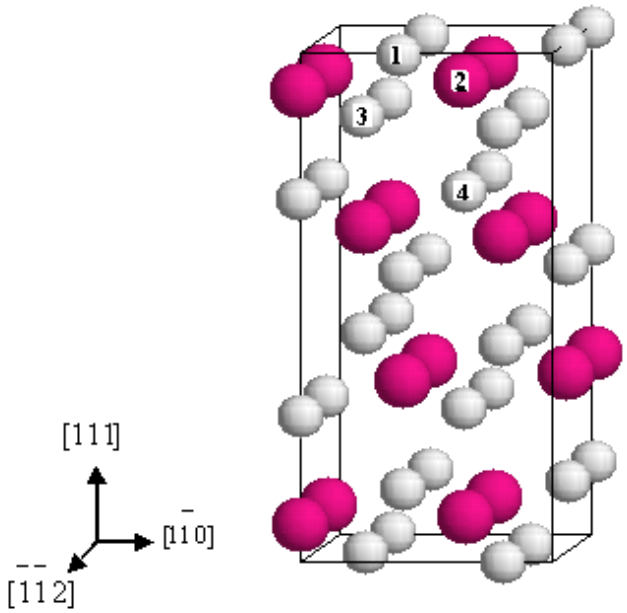

Figure 3.1: Slab model used for ceria (111) surface system. The red and white spheres represent Ce and O atoms respectively. Slabs are repeated in *z* direction and are separated by vacuum layers of 20 Å thickness. Atoms numbered as 1, 6 and 8 are oxygen atoms removed to study the reduced surface energetics of slab at first, second and third layer from surface respectively.

Atomic structure and energetics of the reduced (111) surface

By removing an oxygen atom from ceria, a vacancy site will be created. As a result of the oxygen vacancy, an electron is believed to localize on cerium ions neighboring the vacancy site in a 4*f* orbital, thereby reducing the cerium ions from Ce^{4+} to Ce^{3+} ions. Several experimental studies have imaged the reduced (111) surface using scanning tunneling microscopy (STM) Ref. [40, 41]. One of the important conclusions of these studies, which include an analysis using DFT methods, is that oxygen vacancies tend to group into clusters Ref. [40]. For the present study, however, we will treat only the case of isolated oxygen vacancies. Nevertheless, due to the

limited size of the simulation cell (see Fig. 3.1), in fact the apparent vacancy concentration is quite high. However, we do not consider vacancy clusters as was done in Ref. [40].

Table 3.2: The vacancy formation energy for ceria (111) slab

Position of O-Vacancy	O-vacancy formation energy (in ev)	
	Ref [a]	This work
First layer	3.98	3.36
Second layer	3.80	3.24
Third layer	3.96	3.36

[a] Yang and *et al* [32].

As in Ref. [32], we consider removing a single oxygen atom each of the first three oxygen layers. In particular, referring to Fig. 3.1, the oxygen ions removed correspond to ion 1 for the outermost layer, 3 for the second layer, and 4 for the third layer. We compute the vacancy formation energy from the equation

$$E_{vac} = E(CeO_{2vac}) + 1/2E(O_2) - E(CeO2) \quad (3.1)$$

The results of this calculation are shown in Table 3.2 along with a comparison to prior theoretical results. The differences between our results and the prior results of Yang *et al* [32]. are due to the fact that we did not fix the positions of the bottom six layers in the slab. We found that the relaxations in these layers in some cases were substantial, indicating that relaxations may propagate far into the bulk. We found that our trend of vacancy formation energy is same as that of Yang *et al* [32]. Finally, we also explore creating a vacancy at equivalent sites both on the top and bottom of the slab. We found very little effect, indicating that a single vacancy was sufficient for our study.

One of the most striking results that was not noted specifically in Ref.[32] is the extremely large outward relaxation of the oxygen ion just below the vacancy at the first layer of oxygen on the surface. In fact, it is apparent that when an oxygen vacancy is created in the first or outermost layer of oxygen, an oxygen ion from the layer below relaxes until it actually occupies a position further out than the first layer of cerium ions. In this respect, the resulting structure is in similar to the structure that results when the oxygen vacancy is created in the second oxygen layer. However, the structures are in fact different as can be seen in Fig. 3.2.

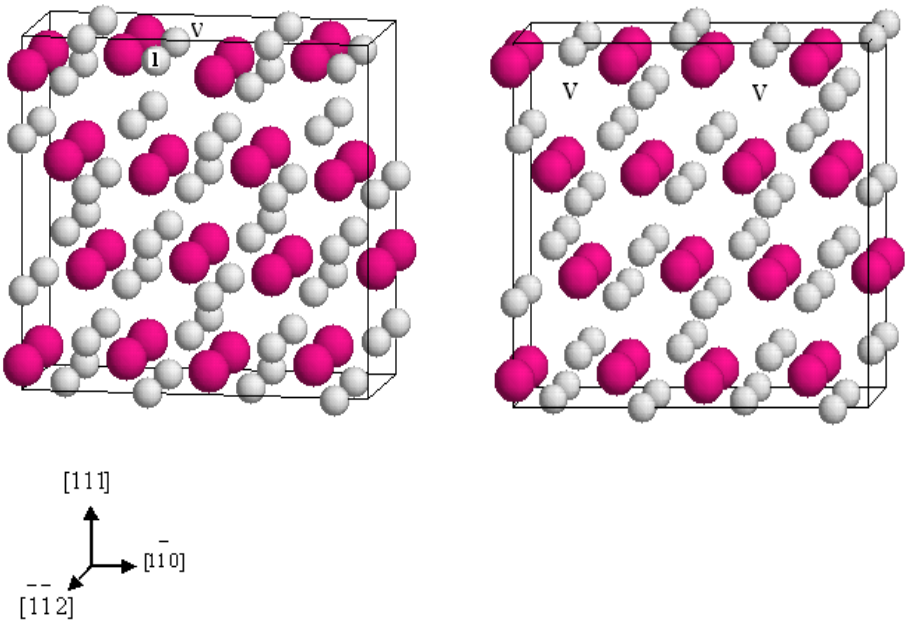

Figure 3.2: Slab models obtained after the relaxation of reduced ceria (111) surface formed by the removal of the oxygen atom present in first layer and second layer. The red and white spheres represent Ce and O atoms respectively: (a) relaxed slab with surface vacancy. 'V' denotes the actual O-vacancy position and atoms numbered as 1 are the O-atoms which relaxed towards surface from second layer, (b) relaxed slab with vacancy in the second layer. Actual positions of the vacancies are denoted as 'V'. Slabs are repeated in *z* direction and are separated by vacuum layers of 20 Å thickness.

Water adsorption at stoichiometric ceria (111) surfaces

Water adsorption on the stoichiometric (111) surface is expected to occur above the cerium ions, with the Ce-O bond between the surface and the water molecule having a length comparable with the Ce-O bond length in bulk ceria. As noted by Henderson and coworkers [12], there are three possible configurations for the water molecule to adsorb on ceria (111) surface. We show the possible configurations schematically in Fig. 3.3. One possibility is that water may adsorb with the hydrogen atoms pointing directly out from the surface. This configuration, which has been called C_{2V} symmetry in the reference to the point group symmetry of the H_2O molecule, was suggested by Henderson *et al* [12] to be most likely adsorption geometry. In this case, the symmetry axis of the water molecule is coincident with the [111] surface normal. However, there is no symmetry argument that favors this geometry. In particular, the symmetry of the ceria surface itself corresponds to a C_{3V} point-group symmetry. As a result, a water molecule adsorbed in the so-called C_{2V} geometry will experience a different environment for each of the two hydrogen ions. It is therefore seems likely that the symmetry axis of the H_2O molecule will tilt somewhat away from the [111] surface normal. If the tilting is significant, the possibility exists that the water molecule will form one or two hydrogen bonds with surface oxygen ions. These two cases are also shown in Fig. 3.3.

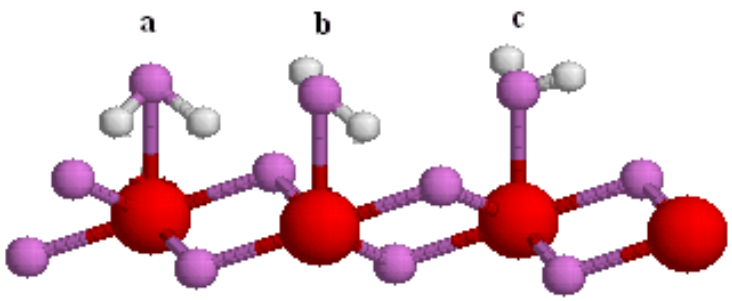

Figure 3.3: Ball-and-stick model of CeO_2 (111) surface, viewed from the side, with absorbed water above Ce ion with different possible geometries of water depending on the possibilities of hydrogen bonding with surface O ion sites. The red, violet and white spheres represent Ce, O and H atoms respectively. Configuration (a) shows possibility of two hydrogen bonds with both the H-atoms of attached water pointing towards surface O ions. Configuration (b) shows possibility of one hydrogen bond with one of the H-atom of attached water pointing towards surface O ion and configuration (c) shows possibility of no hydrogen bond as none of the H-atom of attached water is pointing towards O-ions of surface. [12].

Using several different initial configurations we have shown conclusively that a single hydrogen bond is favored over the C_{2V} geometry and also over the case of two hydrogen bonds. We found in fact that for starting configurations corresponding to geometries 'a' and 'c' in Fig. 3.3 were not stable with respect to forming a single hydrogen bond. For example, beginning with no hydrogen bonds for the C_{2V} geometry, the water molecule tilts downward to form single hydrogen bond. As noticed previously, this is possible because the surface itself does not share the C_{2V} symmetry of the water molecule, resulting in an inequivalent environment for the two H ions. Similarly, a starting structure with two hydrogen bonds spontaneously breaks one of the hydrogen bonds to lower the energy of a single hydrogen bond. Because our simulation was a T

= 0K study, these processes occur without any activation barrier. As a result, it is not possible to compute meaningful adsorption energy for the configurations ‘a’ and ‘c’ of Fig. 3.3.

We nevertheless find some small variation in the water adsorption energy on the stoichiometric (111) surface with the different starting structures. For example, the relative energetics and bond lengths of hydrogen bonds formed between the hydrogen and surface oxygen of these three geometries are shown in Table 3.3. In Fig. 3.4 we show a model of 0.5 Monolayer (ML) of water adsorbed on the stoichiometric (111) surface of ceria with all three possible initial configurations discussed above. All final structures have only one H-bond between a water molecule and O atom at ceria surface but if we look carefully we find that there are two different O atom positions available (numbered ‘1’ and ‘2’) at the ceria (111) surface which can form H-bond with water molecules. These two positions would be identical in a larger system but it can’t be considered identical for our system because of finite size of simulation cell. The observed differences in the adsorption energies of configuration ‘a’ and ‘b’ is due to this finite size effect as H atom of water molecule in configuration ‘a’ is bonded to O atom at position ‘1’ on ceria surface where as that of configuration ‘b’ and ;c’ is bonded to O atom numbered as ‘2’ on the ceria surface. The difference in energetics of configurations ‘b’ and ‘c’ is not a real difference in the energetics as configuration ‘c’ could further be relaxed down to the configuration ‘b’.

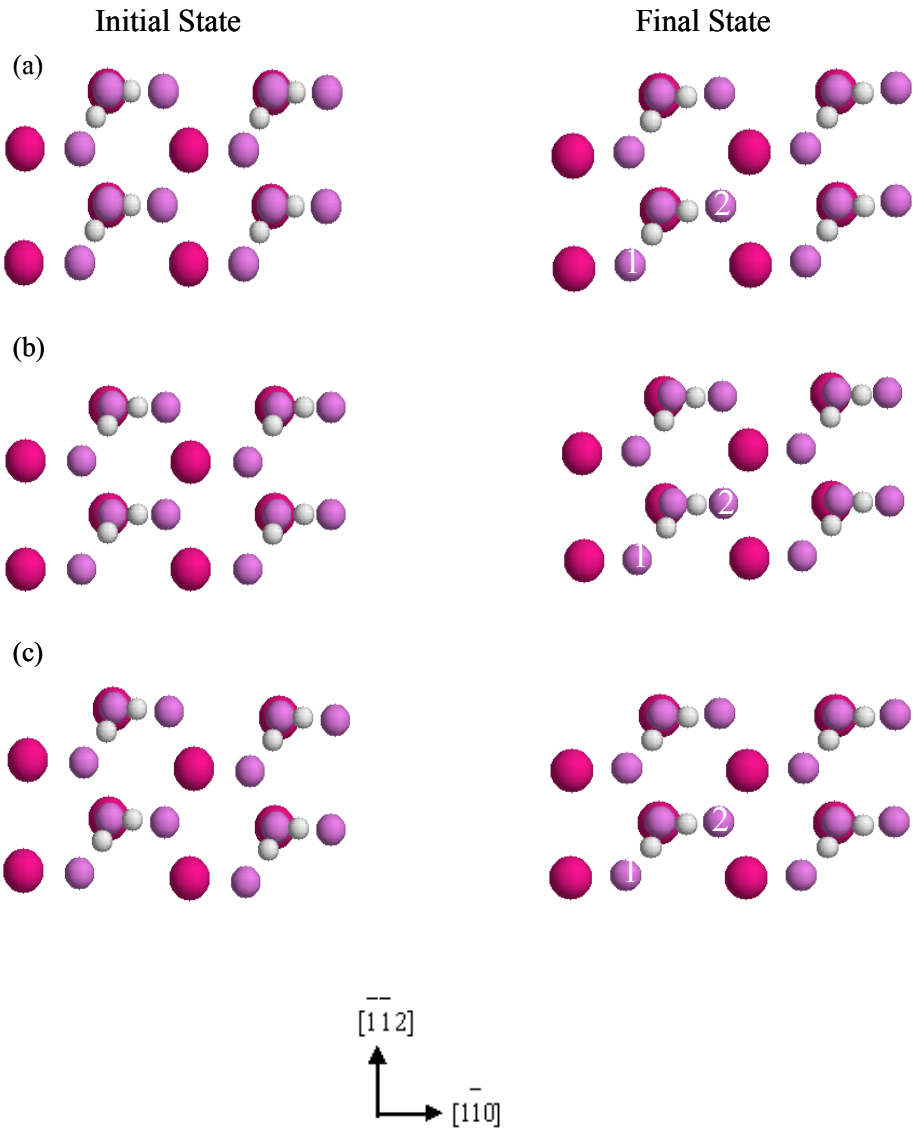

Figure 3.4: A model of 0.5 ML water molecules adsorbed on CeO_2 (111) surface, viewed in the direction of [111]. The red, violet and white spheres represent Ce, O and H atoms respectively. Initial structures (a)-(c) show the possibilities of different degree of H- bonding with O-ions at surface. Final structures (a)-(c) show the actual H-bonding (i.e. only one in each case) in the relaxed structure. For clarity only surface atoms of the CeO_2 is shown.

Table 3.3: Energy of adsorption of 0.5ML of water molecule on ceria (111) surface along with H-bond length in different initial water configurations depending upon the possibilities of degree of H-bonds formations. Finally, in all three cases only one H-bonds formed.

Possible initial water configurations depending upon the possible number of H-bonds	Water adsorption energy (in *eV*)	H-bond length (in Å)
Two	0.562	1.942
One	0.576	1.737
None	0.573	1.814

The computed adsorption energy can be directly related to the Temperature Programmed Desorption (TPD) experiments using Redhead analysis [42, 43] as done by Henderson *et al* [12]. The Redhead analysis is used to interpret experimental studies of desorption of species adsorbed on a surface with the temperature of the system increased at a constant rate. Assuming a constant heating rate, the activation energy can be determined from the Redhead equation [43]:

$$E/RT_p = \ln (\nu T_p/\beta) - C \qquad (3.2)$$

where T_p is the temperature at which the desorption rate is maximum, E is the activation energy of desorption, ν/β is pre exponential factor which is taken as 10^{13} S^{-1} as a typical vibrational frequency[42, 43]. We show for comparison the experimental results in Table 3.4. The good agreement is an indication that the DFT results are providing a realistic description of the system. However, the exact coincidence of the theoretical and experimental results should not be taken too seriously. The DFT results are probably only accurate to within a few tenths of *eV*.

Furthermore, the simple theory used to determine energetics based on desorption kinetics is very approximate. In short, the nearly exact agreement between theory and experiment is fortuitous, and more importantly the rather small differences between the simulated energies of the three possible binding modes makes it impossible to determine the particular adsorption geometry based on a comparison of experimental and theoretical results as these differences are again due to the finite-size effect of our simulation cells.

The most notable feature of the experimental results is the presence of fairly strong coverage-dependent desorption energy especially when the surface is nearly stoichiometric. There are different possible explanations of this effect. For example, because the water forms hydrogen bonds at the surface, competition for the bonding sites represent a possible mechanism. This, however, only seems likely in the event that two hydrogen bonds are formed for each adsorbed water molecule. In particular, each cerium ion at the surface is coordinated with three surface oxygen ions. However, each of the surface oxygen sites is shared by three surface cerium ions. As a result, in the instance that water molecules form double hydrogen bonds with the surface, all available oxygen sites will be saturated at 0.5 ML coverage. Because we predict single hydrogen bonds, it is possible to have 1.0 ML coverage without competition for available oxygen sites. Based on our results, therefore competition between available sites seems an unlikely explanation for the experimentally observed coverage dependence.

Another possible explanation for the coverage-dependence in the experimental TPD results is the increasing importance of dipole-dipole interactions as the coverage increases. To explore possibility, we studied the energetics of a complete monolayer of water adsorbed to the surface. The second water molecule was added in different starting configurations to a structure with 0.5 ML of water already adsorbed with single hydrogen bonds with the surface. As with the

0.5 ML case, we find that it is energetically favorable for each adsorbed water molecule to form a single hydrogen bond at the surface. This result was independent of the starting configuration of the second water molecule added to the surface. While the adsorption energy of the second water molecule is less than that of the adsorption energy of the first water molecule, the difference was very small. In particular, the differences are much too small to explain the experimental coverage dependence. The adsorption energy of second 0.5 ML water molecule on ceria (111) surface which already have 0.5 ML of water molecule attached to it is shown in Table 3.4 along with dipole-dipole interaction of water molecules on ceria (111) surface. We note that long-range dipole-dipole interactions are not described by the periodic boundary conditions. In particular, while it is energetically favorable for nearby water molecules to have parallel dipole moments, over longer length scales we would expect domains to form to reduce the energy associated with the macroscopic electric field created by presence of the oriented dipoles.

Initial possible structures and final relaxed structures of ceria (111) surface with 1.0 ML of water adsorbed on the surface are shown in Fig. 3.5a-c.

Table 3.4: Adsorption energy of 0.5 ML of water molecule on ceria (111) surface which already have 0.5 ML of adsorbed water molecule on its surface. Here again all three different initial water configurations are considered depending upon the possibilities of degree of H-bonds formations. Experimental value is also shown for comparison.

Possible initial water configurations depending upon the possible number of H-bonds *	Adsorption energy (in *eV*)	Dipole-dipole interaction energy (*eV*)
Two	0.553	0.038
One	0.542	0.038
None	0.543	0.038
Expt [12]	0.53	____

* Finally, in all three cases only one H-bonds formed between hydrogen of water and O ion of ceria (111) surface.

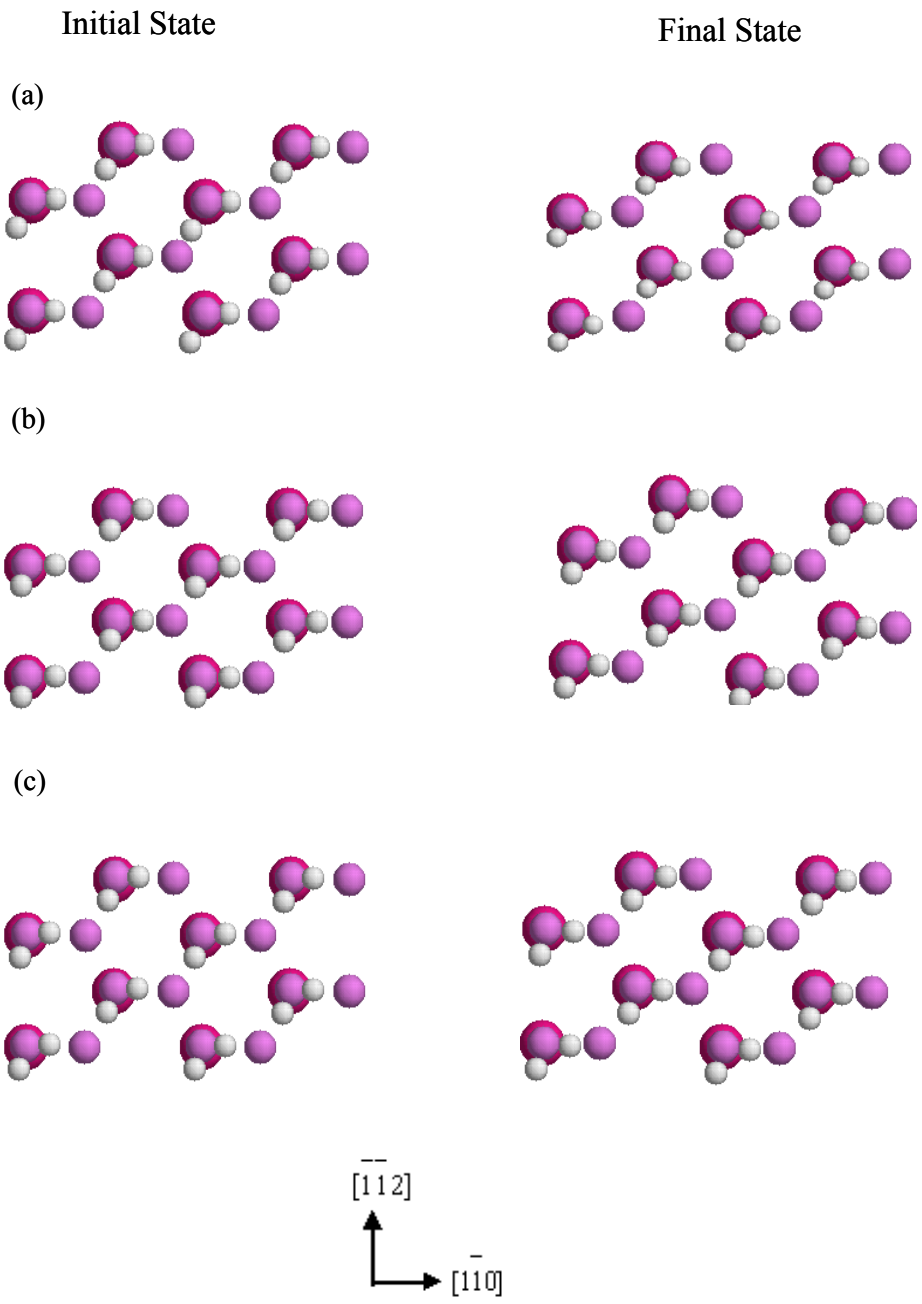

Figure 3.5: A model of 1.0 ML water molecules adsorbed on CeO_2 (111) surface, viewed in the direction of [111]. The red, violet and white spheres represent Ce, O and H atoms respectively. Initial structures (a)-(c) show the possibilities of different degree of H- bonding with O-ions at surface. Final structures (a)-(c) show the actual H-bonding (i.e. only one in each case) in the relaxed structure. For clarity only surface atoms of the CeO_2 is shown.

Water adsorption at the reduced ceria (111) surface

The presence of oxygen vacancies is expected to increase the adsorption energy of water. This is due to the fact that under coordinated Ce ions will have more electrons available for binding. Another important consideration is that oxygen vacancies are in some sense comparable to positively charged sites, and as such will tend to attract negative ions. In short, there should be an effective attractive interaction between water molecules and oxygen vacancies. However, it is not clear whether oxygen vacancies at the surface and water molecule form a stable complex or not. It may be that water will oxidize the surface, thereby eliminating oxygen vacancies with evolution of hydrogen gas. In several prior experiments, this behavior was in fact directly observed at the temperature of 500 to 700 K [8-10], including for water at the (111) reduced surface. On the other hand, more recent experiments suggest, at least for the (111) surface, that oxidation of the reduced surface does not occur [12]. Instead presence of water at the interface results in an apparent increase in the further reduction of the surface [12].

We have studied several possible configurations of water molecule on ceria surfaces in the proximity of a single oxygen vacancy in either the first, second, or third oxygen layers. We have considered several different initial positions of the water molecule on the defective surface, including directly above the cerium ion nearest to the vacancy, and also directly above the vacancy. We overwhelmingly find that the water molecule prefers to be adsorbed directly above the cerium ion rather than above the vacancy site. In Table 3.5 we show the adsorption energy of the 0.5 ML of water on reduced ceria (111) surface for different O-vacancy positions. In each case, the geometry of the adsorbed water molecule represents the lowest energy state given the particular location of the oxygen vacancy. Confirming our expectations, we find that the oxygen

vacancy does in fact tend to increase the adsorption energy. In Fig. 3.6a-d we have shown the relaxed structures of water adsorbed on the different defective ceria (111) surfaces.

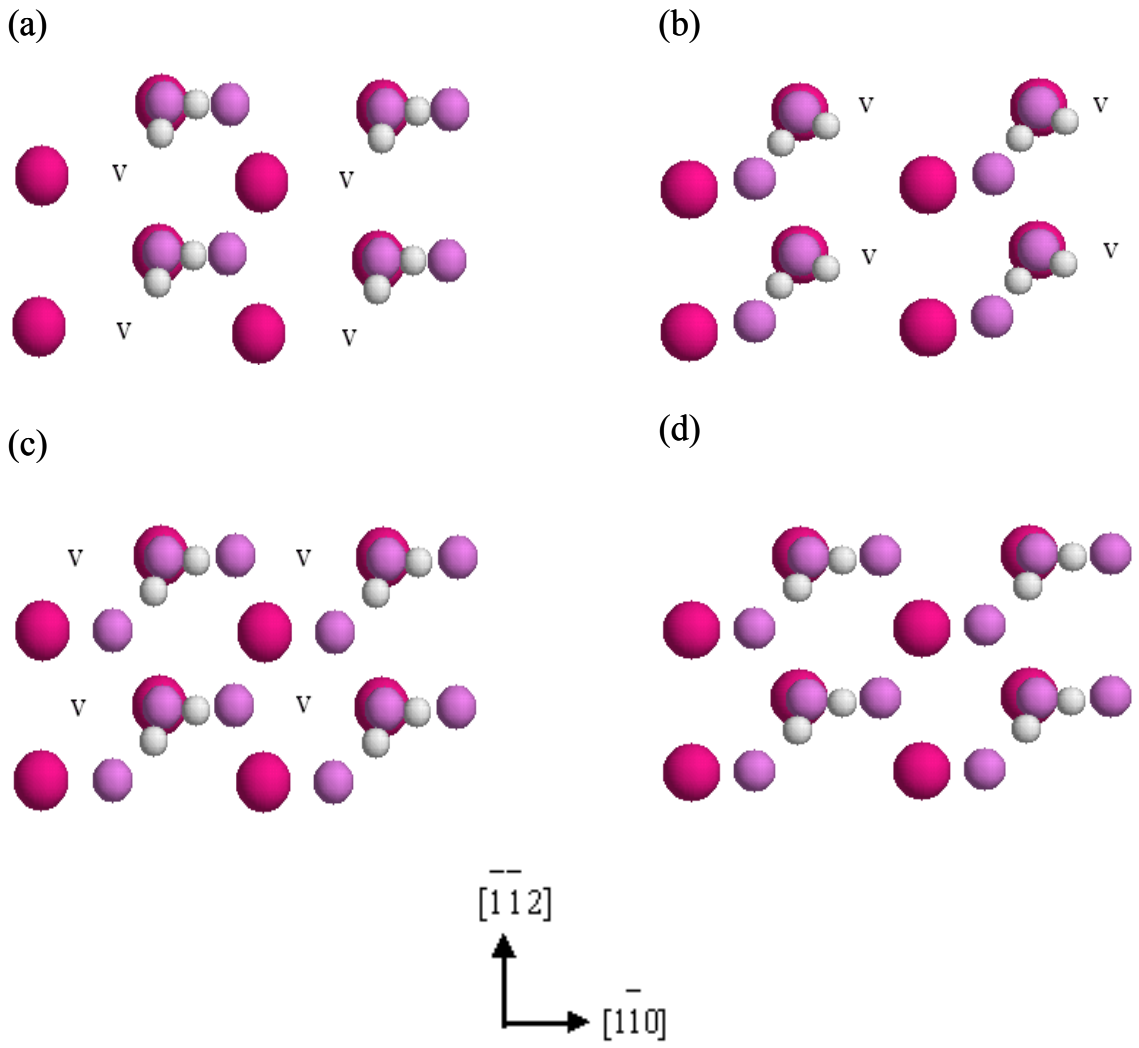

Figure 3.6: A model of 0.5 ML water molecules adsorbed on the different reduced CeO_{2-v} (111) surface, viewed in the direction of [111]. The red, violet and white spheres represent Ce, O and H atoms respectively. Structures (a)-(d) show the actual H-bonding (i.e. only one in each case) in the relaxed structures with O-vacancies at the first, first (with O vacancy at another site), second and third layers respectively. For clarity only surface atoms of the CeO_2 is shown.

Table 3.5: Adsorption energy of 0.5 ML of water on reduced (111) ceria surface with different positions of O-vacancies.

Positions of O-vacancies	Adsorption energy of water molecule (in ev)
First layer	0.64
Second layer	0.61
Third layer	0.72

A direct comparison of the results in tables 3.3 and 3.5 shows that the adsorption energy of the water molecule is increased by the presence of the oxygen vacancy. The strongest adsorption energy occurs when the oxygen vacancy is in the third layer from the surface and water molecule is adsorbed on the cerium ion directly above the oxygen vacancy. In this geometry, the adsorption energy in 0.72 eV which is minimum amount of energy that needs to be added to the system to cause desorption of water molecule with the position of the oxygen vacancy left unchanged after desorption. However, while the adsorption energy is strongest in this case, it is not the lowest energy structure. The ground-state structure for an adsorbed water molecule occurs when the oxygen vacancy is in the second layer from the surface. The reason for this is due to fact that the oxygen vacancy formation energy is smallest for the second layer of oxygen ions. Therefore, while the attractive interaction between the oxygen vacancy and the water molecule is strongest when the oxygen vacancy is in third layer, it takes significantly less energy to create oxygen vacancies in the second layer. The difference in the ground state energies of these two structures is 0.01 eV, which is in fact quite small and may be beyond the

accuracy of the DFT method used here. However, if the difference is in fact very small as our calculation suggests, it is then likely that when water is adsorbed at the surface, oxygen vacancies will be observed in significant numbers both in the second and third layer of surface. For the case of water adsorption with oxygen vacancy in the first layer at the surface, energy is significantly (~0.08 *eV*) higher when compared to the ground-state structure. However, this is still small enough that at room temperature a significant number of water molecules will adsorb near oxygen vacancies on the first layer.

We next consider the relative increase of oxygen vacancies at the surface which should occur in the presence of adsorbed water. This phenomenon has been observed previously in experiment [12]and interpreted to be due to the effective attraction between vacancies and adsorbed water molecules. To estimate the relative increase in concentration of vacancies at the surface, we need formation energy of vacancies in the bulk. This has been previously computed using DFT to be 4.73 *eV* [32] and we calculated the vacancy formation energy at the (111) surface in the presence of water to be 3.21 *eV* according to the following relations

$$E\ (CeO_{2,vac}+H_2O_{adsorbed}) + \tfrac{1}{2}\ E(O_2) - E\ (CeO_2+ H_2O_{adsorbed}) \qquad (3.3)$$

Then we also have vacancy formation energy at the ceria (111) surface without the presence of water as 3.36 *eV* from Table 3.2. So ignoring the chemical potentials there is a decrease in the vacancies formation energy of ~ 0.15 *eV* at the surface in the presence of water which in other words can cause the relative increase in the concentration of vacancies at the surface in presence of water.

The increase in vacancy concentration at the reduced ceria (111) surface due to presence of water can be accounted in another way like this. As discussed earlier there is increase in the adsorption energy of water on the reduced surface compared to the stoichiometric surface which

indicates an effective attractive interaction between vacancies and adsorbed water molecules. The maximum adsorption energy of water on the reduced ceria (111) surface is computed as 0.723 *eV* where as it is 0.576 *eV* for stoichiometric surface. So there is an increase of 0.147 *eV* in the adsorption energy of water on the reduced surface. This particular reduced surface has O-vacancies directly below the Ce ions to which water is adsorbed at the surface. Viewing the problem in a different way, we could imagine fixing the concentration of water molecules at the surface and then considering what this implies for the concentration of oxygen vacancies at the surface. So taking above mentioned increase in adsorption energy as the decrease in the vacancy formation energy *i.e.* $\Delta E = 0.147$ *eV* we calculated the increase in relative concentration of vacancies to be equal to $2.95X10^2$ at room temperature using exponential dependence of vacancy concentration on the change in adsorption energy as follows $\Delta N = Exp(-\Delta E/k_bT)$. Where, ΔN is the ratio of vacancy concentration at the ceria (111) surface in the presence and absence of water. Here we must keep in mind that we can neglect chemical potential even at room temperature if the concentration of vacancy is small as we are considering the ratio of the vacancy concentration while calculating the change in their relative concentration.

Finally, we have addressed the question of whether water will tend to oxidize the reduced surface. To consider this question, we consider the energy required to oxidize the reduced surface and evolve hydrogen gas (H_2 molecules). In other words, we consider the energetics of the reaction,

$$Ce_8O_{15} + (H_2O)_{ad} \rightarrow 8\ CeO_2 + H_2 \qquad (3.4)$$

Earlier we have calculated the energy of the most stable structure of water adsorbed to the reduced ceria (111) surface as -216.00 *eV*, energy of 8 units of CeO_2 is calculated as -209.25 *eV*

where as energy of hydrogen molecule is -6.80 *eV*. So we obtain an energy of -0.05 *eV* for the water adsorbed to the ceria with subsurface vacancy using following relation

$$E_{reaction} = 8*E\ (CeO_2) + E\ (H_2) - E\ (Ce_8O_{15}\text{---}\ H_2O) \qquad (3.5)$$

but we don't have any experimental results to compare with. We find that the reaction is weakly exothermic, indicating that in fact oxidation will proceed. However, it is not entirely certain that this small energy difference can be accurately resolved by DFT methods. As a result, we are not certain that the oxidation reaction should be expected to proceed based on this result. Another possibility is that the low-energy structure we found for water adsorbed on the defective surface is not the true ground state. To help identify a potentially lower energy structure, we attempted to determine the stability of our system using finite-temperature MD simulation. Starting with CeO_2 structures which have a vacancy and water adsorbed to the surface, we begin an MD simulation at a temperature T = 300K. The simulation was continued for 0.6*ps*, then cooled to T = 200K for 0.3*ps*, then again the temperature was decreased to T = 100K and the MD simulation were continued for 0.25*ps*. Finally the system was cooled to T = 0K and relaxed, after relaxation we found that one hydrogen bond configuration is indeed the lowest energy state. In Fig. 3.7 we have shown one such structure obtained after MD as discussed above.

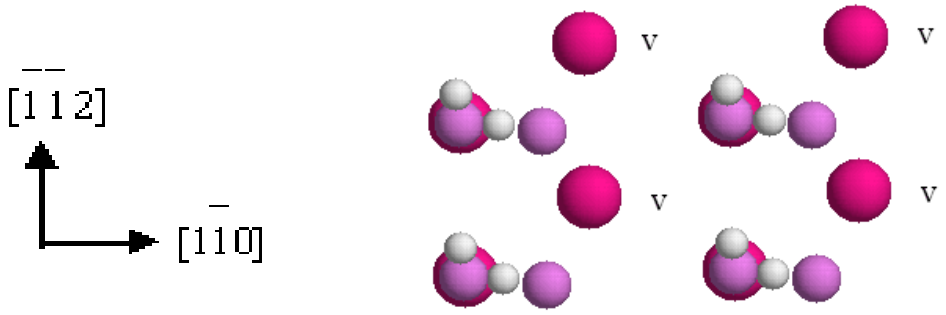

Figure 3.7: A model showing a water molecule adsorbed on the reduced ceria (111) surface after MD. The red, violet and white spheres represent Ce, O and H atoms respectively and for clarity only surface atoms of the ceria (111) are shown.

Finally, an important consideration apart from the overall energetics is reaction kinetics. In particular, we note that for oxidation of the surface to occur, the bonds in the water molecule must be broken and the oxygen ion from the water inserted into the defective lattice. The structures obtained for surface oxygen vacancies suggest the possibility that this may be difficult to do. In particular, oxygen vacancies like to exist below the surface oxygen layer. This suggests that perhaps surface oxygen must first hop into vacancy sites in the sub-surface layer before oxidation of the lattice can occur. This may involve a significant activation barrier that prohibits oxidation at room temperature.

Discussion and Summary

As discussed before one important shortcoming of DFT methods, including both GGA and LDA functionals, is in the treatment of localized electronic states. In particular, because the Hartree method alone does not correct for self-interactions, the exchange-correlation functional alone approximately corrects for the self interactions. It is expected, however, in many cases that self interactions may not be correctly accounted for within the GGA or LDA. This may result,

for example, in a poor description of electronic screening of oxygen vacancies in reduced ceria. In particular, the *f*-electronic orbitals on the cerium ions lie lower in energy than the other valence electrons, and are also usually thought to have very localized orbitals. This has led, for example, Skorodumova *et al* [44] to suggest that a more accurate approach to understanding the reduction of ceria is to place the electrons freed by removing an oxygen atom for a stoichiometric system into localized f-orbitals on two neighboring cerium ions [44]. If indeed the electrons that screen oxygen vacancies are localized in this way, it is likely to have profound implications for the present study. However, we do not know of any first principles approach to estimate this affect. Nevertheless, these observations point to the need for improved DFT functionals for studying localized electronic states. Another approach that might be useful is to apply a mixed Hartree-Fock and DFT method such as the popular BLYP approach. The advantage of this approach is an improved correction for the self-interaction term.

One of the difficulties in applying standard DFT techniques is that the exchange-correlation functionals apparently do not correctly describe the localization of electrons at metal ions. This problem is probably due to the fact that self-interaction is incorrectly included. For ceria, this problem may have even more important effect especially while dealing with defects. One approach that has been applied is to treat differently the cerium ions near a vacancy site as in LDA + U.

CHAPTER 4 : WATER MODEL USING SIESTA

Introduction

Classical models of water, that use empirical pair potentials, have for some time now been used successfully to describe the structure and dynamics of water [45-48]. One advantage of classical models is that they can overcome the length and timescale limitations of first-principles methods. The accuracy and realism of the models have been greatly improved from the original rigid molecule approach [47]. More realistic models account for not only internal vibrational modes of the molecule, but also electronic polarization [45, 46]and dissociation[45]. However, there still exist many problems where an ab initio approach is desirable or even essential. For example, realistic modeling of modeling of ionic solutions [49]or chemical reactions is often not possible with classical methods.

First-principles models of liquid water on the other hand can describe dissociation, reaction, and ion solvation. However, it has still proven to be a challenge to obtain accurate results using DFT methods. For example, calculations within the LDA for the exchange and correlation functional are known to grossly overestimate water-dimer binding energies [50, 51]. As a result, the structure of liquid water is not at all accurately described by LDA. On the other hand, gradient correlation to the exchange-correlation functional has yielded much better agreement with experiment [51-53]. Overall, first-principles simulations seem to result in a somewhat overstructured liquid with self-diffusion coefficients that are in significant disagreement with experiment. While the agreement with experiment is certainly adequate for

many applications, first-principles simulation of liquid water is computationally very intensive. At the present time, simulations are limited to about 100 molecules and times on the order of 10*ps*. This provides the motivation for developing new and more efficient computational approaches that still retain the accuracy of traditional DFT calculations.

One promising approach is to develop electronic-structure methods that utilize limited basis sets. For example, Ortega and coworkers [54] have already successfully applied a linear combination of atomic orbitals (LCAO) approach to liquid water. The SIESTA method also employs a local basis set of atomic orbitals and has been developed to incorporate an approximate O(N) algorithm for large-scale simulation [55-57]. There have been two extensive applications of SIESTA to problems involving water [58, 59]. For example, a recent article describes the use of SIESTA to compute the optical conductivity of DNA molecules in the presence of water [59]. Another recent article investigated water adsorption and dissociation at alumina clusters using SIESTA [58] However, there has not yet been a systematic study of the application of SIESTA to bulk liquid water. A systematic study is a necessary first step to assess the ability of SIESTA to treat problems involving liquid water.

In this work, we have studied the application of SIESTA to liquid water. We established that by varying the basis set (i.e. the atomic orbitals) to accurately reproduce the structure and energy of isolated water dimers, a reasonable model for liquid water can be realized. Three different basis sets were extensively tested in molecular-dynamics (MD) simulations of liquid water, and the resulting radial-distribution functions are compared to experimental neutron scattering data.

Computational Approach

As discussed earlier SIESTA's accuracy is compromised in comparison to other ab initio methods which typically use plane-wave basis set. However, it has been shown that the addition of more basis states improves the accuracy of the SIESTA method [60]. However, increasing the size of the pseudo-atomic orbital (PAO) basis has the important disadvantage of increasing the computational load, and basis-set optimization should always be considered as a first step.

The SIESTA method provides a simple and flexible approach to generate basis sets. The approach used is to solve the electronic-structure problem for an isolated atom with a spherically-symmetric confining potential to localize the atomic orbitals. A similar approach was used in the LCAO method developed by Sankey and Niklewski [61]. In local-basis set methods, the Kohn-Sham wave functions are expanded as linear combination of PAOs as.

$$\left|\phi_i(\vec{r})\right\rangle = \sum_{\mu\alpha} \alpha_i^{\mu\alpha} \left|\varphi_\alpha^{PAO}(\vec{r} - \vec{R}_\mu)\right\rangle \qquad 4.1$$

where index α represents all the valence orbitals on a single atom. Another requirement imposed on the form of PAO is boundary condition that it should vanish outside some predetermined radius r_c.

$$\varphi^{PAO}(\vec{r})\,|_{r=r_c} = 0 \qquad 4.2$$

which has the physical effect of mixing in slight amounts of excited orbitals of atoms inside r_c. This condition limits the spatial extent of PAOs thereby resulting in a sparse Hamiltonian matrix.

The confining potential is described by the equation:

$$V(r) = V_o \exp[-(r_c - r_i)/(r - r_i)]/(r_c - r) \qquad 4.3$$

which depends the three parameters r_i, V_o and cutoff radius r_c [60, 62]. A typical confining potential is shown in Figure 4.1. The PAOs generated in this way serve as basis states for application to, for example, studies of isolated molecules, crystals, or liquids.

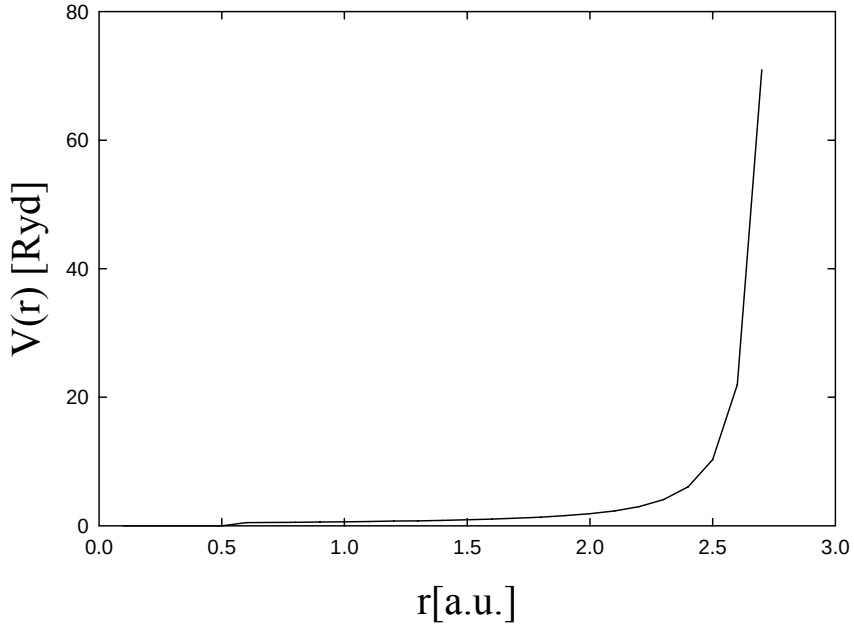

Figure 4.1: A typical confining potential V(r) for generation of PAO basis states. The parameters r_c, r_i, V_o used in this figure correspond to a confining potential used in our work for 2s orbitals for Oxygen.

A useful parameter to characterize the PAO basis is the orbital energy shift ΔE_{PAO} [62]. This parameter is determined by computing the difference between the energy of an atom computed using the confined PAO basis and the exact ground-state energy. Because the confined orbitals are different than the exact ground-state orbitals, the energy of the atom computing using the PAO basis is expected to be greater than the ground-state energy, and hence ΔE_{PAO} is always non-negative. Other physical properties can depend significantly on the particular basis used in a calculation. However, it has been shown previously that fairly systematic convergence to

physical quantities can be obtained by varying the energy shift ΔE_{PAO} [62]. For our description of liquid water, we have taken the approach of computing physical parameters including the dimer binding energy, liquid structure and density, as a function of the PAO basis sets that span a wide range of ΔE_{PAO}. If the properties of interest are found to depend in a systematic way on ΔE_{PAO}, it is likely that a robust approach can be developed to identify improved PAO basis sets without having to resort to application of a larger basis set.

For our studies, we used the SIESTA codes with a double- ς PAO basis. As described below, several basis sets covering a wide range of values of ΔE_{PAO} were considered. The so-called second- ς of the PAO basis is chosen to reproduce the tail of the first-ς PAO, but for r < R_{DZ} smoothly continues to the origin as $r^l(a - br^2)$, where l is the angular momentum channel and *a* and *b* are chosen to ensure that the basis state is continuous and differentiable at r = R_{DZ} [62]. We have also included polarization orbitals which in SIESTA are determined from perturbation theory applied to the first-ς orbital [62]. The different PAO basis sets were tested for their ability to reproduce the properties of isolated water molecules, water dimers, and the structure and dynamics of liquid water. We used the Beck-Lee-Yang-Parr (BLYP) functional to treat electron exchange and correlation within the generalized-gradient approximation (GGA) [63, 64]. We used Troullier-Martins norm-conserving pseudopotentials [65] in the Kleinman-Bylander form [66]. The 1s electrons for oxygen were treated as core electrons. All of the remaining electrons for hydrogen and oxygen were treated as valence electrons.

Results for isolated molecules and water dimers

As the structure of liquid water is very sensitive to the strength of the hydrogen bonds, we first tried to develop an optimized basis by considering the dependence of the water-dimer binding energy on the choice of PAO basis. We computed the dependence of the water-dimer binding energy on ΔE_{PAO} for several PAO basis sets. In Fig. 4.2, we show that the binding energy of the water dimer depends in a systematic manner on ΔE_{PAO}. The distance r_{OO} between the oxygen ions in the dimer is shown in Fig. 4.3 to also depend systematically on ΔE_{PAO}. Interestingly, while the dimer binding energy varies by a factor of about 3 over the range of ΔE_{PAO} considered the values of r_{OO} change only slightly. The experimental values for the dimer binding energy and r_{OO} are 5.4 ± 0.7Kcal/mol [67, 68] and 2.98 Å [69, 70] respectively. Figure 4.2 shows that it should be possible to adjust the basis set to achieve good agreement with experiment for the dimer binding energy. On the other hand, the large experimental uncertainty also indicates that a direct fit to experiment may not be practical. For the oxygen-oxygen separation r_{OO}, our values are near to the experiment but consistently somewhat smaller. Overall, comparison of our results with experiment suggests that we should be able to identify a basis set which provides an adequate description of the water dimer. Because the hydrogen bonds play a fundamental role in the structure of liquid water, it seems likely that a model which describes the water dimer correctly will also be useful for simulations of liquid water.

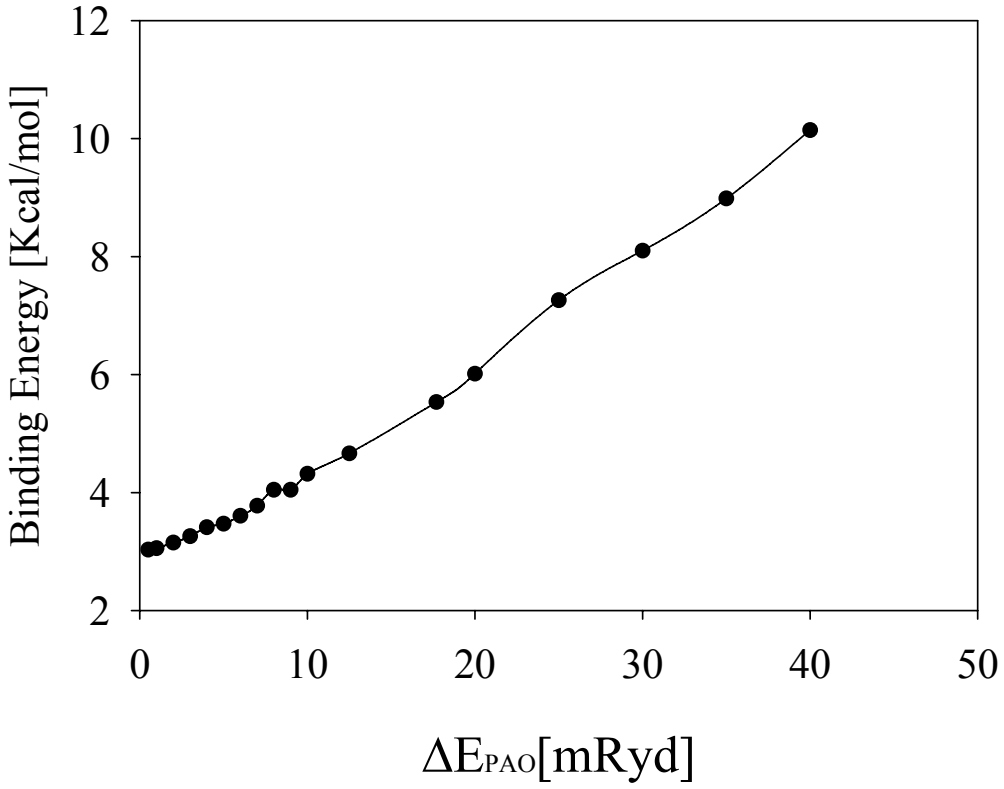

Figure 4.2: Binding energy for water dimers determined as a function of ΔE_{PAO} for different PAO basis sets.

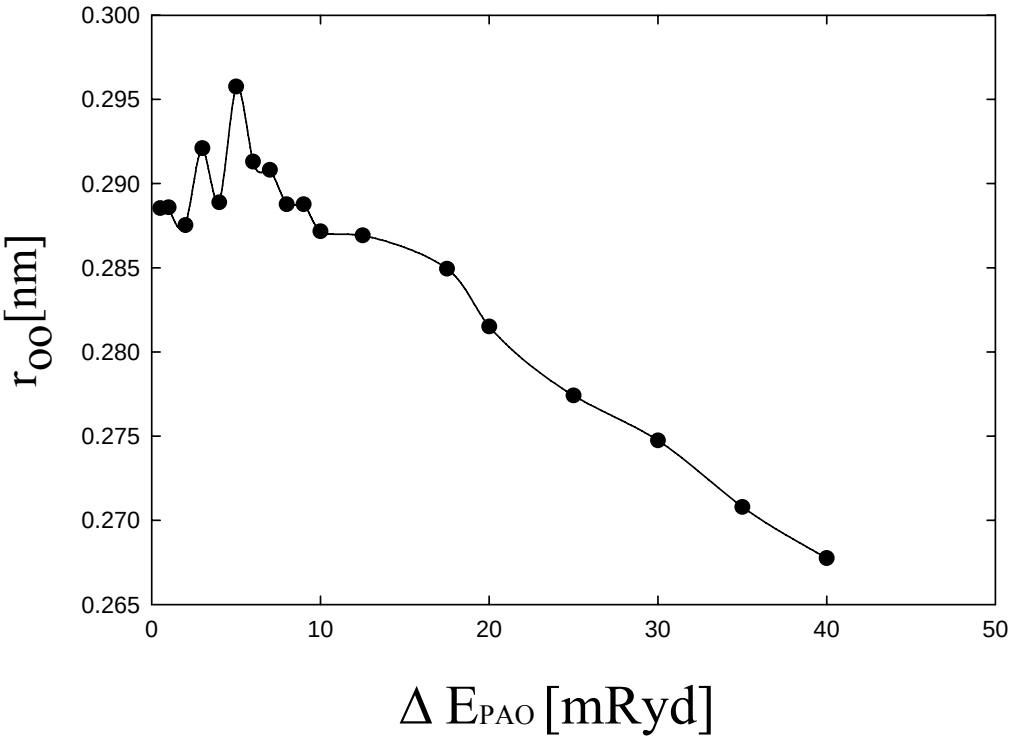

Figure 4.3: Dependence of the distance r_{OO} between the oxygen ions in the water dimer on ΔE_{PAO} for several different basis sets. The behavior becomes somewhat irregular for ΔE_{PAO} values below 8.0 *mRyd*. Values of r_{OO} are consistently somewhat less than the experimental value of 2.98 Å from ref [70].

While the properties of the dimer are critical, it is equally important that the properties of an isolated water molecule are accurately reproduced by the PAO basis. We have found that the properties of the isolated water molecule are in fact fairly insensitive to the PAO basis. Considering observations by other groups, this may not be very surprising. For example, while the LDA grossly overestimates the binding energy of water dimers, and results in a description of liquid water that is very unrealistic, the LDA actually does quite a reasonable job of describing a single water molecule [51, 53, 60]. Our results indicate, as with the particular choice of the exchange-correlation functional, that the choice of basis set does not strongly affect the

properties of a single water molecule. This fortuitous result permits a significant amount of freedom in tuning the basis set to result in optimized properties of the water dimer without simultaneously destroying the ability to predict accurately the properties of a single water molecule. For example, in Table 4.1 we show the three vibrational modes computed using SIESTA for different values of ΔE_{PAO}. For each value of ΔE_{PAO}, the calculated vibrational frequencies are in reasonable agreement with experiment [71]. It should be noted that the dependence on ΔE_{PAO} is not monotonic. However, the changes are quite small and the computed frequencies are in all cases reasonably close to experimental observations. We believe that the non monotonic behavior is likely due to small numerical errors that result from, for example, the real and Fourier space grids that are used to compute matrix elements and electrostatic interactions. As with the vibrational frequencies, the bond lengths and bond angles are not very sensitive to the details of the basis set. For ΔE_{PAO} below 12.5mRyd, the oxygen-hydrogen bond length lies always between 0.97Å and 0.99Å. For the same range of ΔE_{PAO}, the bond angle in the isolated water molecule is within 1^o of 105^o. These values are in good agreement with the experimental bond length of 0.957 Å and bond angle of 104.5^o [72, 73]. Furthermore, the results of our SIESTA model are consistent with the values of 0.973Å and 104.4^o found in previous ab initio calculations using the BLYP functional [51]. In summary, through a systematic variation of PAO basis sets, the properties of water dimers, including the binding energy and r_{OO}, can be tuned to within the experimental range. On the other hand, the properties of an isolated H_2O molecule do not strongly depend on the particular basis set. These results suggest that it should be possible to tune the basis set to identify a model which can reproduce the structure of liquid water. In the next section, we test this idea out by performing MD simulations for different choices of PAO basis and compare the results with experimental observations.

Table 4.1: Water vibrational frequencies computed using different PAO basis sets in SIESTA. The frequencies ν_1, ν_2, and ν_3 correspond to the bond bending, symmetric stretch, nad asymmetric stretch modes respectively. Also included is the experimental data from Ref [71].

ΔE_{PAO} (mRyd)	$\nu_1 (cm^{-1})$	$\nu_2 (cm^{-1})$	$\nu_3 (cm^{-1})$
2.0	1493	3687	3831
8.0	1516	3672	3819
10.0	1506	3671	3823
12.5	1518	3662	3812
15.0	1499	3666	3821
17.5	1531	3658	3810
20.0	1550	3660	3814
25.0	1575	3662	3808
30.0	1579	3646	3803
35.0	1611	3656	3799
40.0	1640	3662	3815
Expt [71]	1595	3657	3756

Molecular-dynamics simulations of liquid water

Molecular-dynamics simulations were performed for three different PAO basis sets which correspond to ΔE_{PAO} = 8.0mRyd, ΔE_{PAO} = 10.0mRyd, and ΔE_{PAO} = 12.5mRyd. From the results in Fig.4.2, it can be seen that the dimer binding energy spans significant range of values for these three PAO basis sets. In fact, the dimer binding energy increases smoothly from 4.05 kcal/mol for ΔE_{PAO} = 8.0mRyd to 4.66 kcal/mol for ΔE_{PAO} = 12.5mRyd. These lie somewhat below most accepted experimental values. For example, the experimental range is usually accepted to be 5.4 ± 0.7 kcal/mol [67, 68]. However, theoretical values have typically covered a much broader range from 4.1kcal/mol to 6.1kcal/mol [74]. Because the basis sets considered here result in significantly different dimer binding energies, the simulated properties of liquid water should be strongly dependent on the choice of PAO basis. In each of the simulations described here, we began with a cubic (i.e. diamond lattice) ice structure. The simulation supercell contained 64 H_2O molecules with the initial supercell volume chosen to result in a density of 1.0 g/cm3. Because the periodic nature of the system is an artifact of the finite size of the simulation cell, the electronic structure was computed for only one $\vec{k}$ -point (i.e. $\vec{k}$ = 0)The simulations sampled the canonical ensemble with the temperature controlled by a Nose-Hoover thermostat [75, 76]. The ice structure was then melted at 500K using the constant-pressure algorithm due to Parrinello and Rahman [77] with no externally applied pressure. The melting of the initial ice crystal was performed at 500K for a total time of 0.5ps. After melting at T = 500K, the system was cooled to T = 315K and then simulated for a total time of 6.5ps. The electronic structure at each MD step was determined to within 10^{-4}eV, and so we expect that the system should follow

the Born-Oppenheimer energy surface. The MD time step was chosen to be 0.5fs, which we found to result in energy drifts within a constant energy simulation of less than 10^{-4}eV per MD step. Over the course of a 6.5ps simulation, this drift corresponds to a temperature of about 25K. However, the simulations reported below were performed at constant temperature rather than constant energy, and as a result the temperature and total energy does not exhibit any drifting. The wavefunctions, electron density, and Coulomb and exchange-correlation potentials are defined on a real-space grid. The grid itself can also be defined in reciprocal space. The grid used in our simulations corresponded to an equivalent plane-wave cutoff energy of 200Ryd.

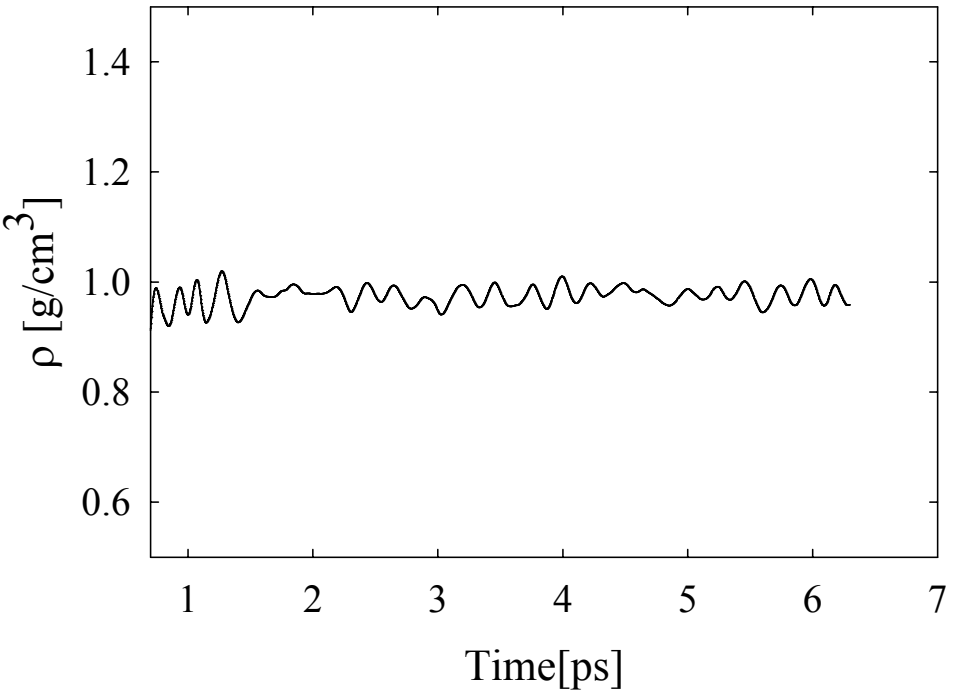

Figure 4.4: Time-dependence of the mass density from an MD simulation of liquid water using the basis set with ΔE_{PAO} = 8.0*mRyd*. The temperature is maintained at T=315*K*. After about 2.5*ps* of MD simulation, the average density appears to be constant and close to the accepted value of 1.0 g/cm^3.

The system was first equilibrated for 2.5ps at T = 315K. In Fig. 4.4, the density of the water is shown as a function of time. There appears to be no significant drift in the density beyond the first 2.5ps of equilibration, indicating that our system is reasonably well equilibrated. In Fig. 4.5 we show the potential energy as a function of time. It can be seen from Fig. 4.5 that the potential energy is not significantly drifting after 2.5ps. This is an indication that the system is reasonably well equilibrated and that time averages computed after the initial 2.5 ps should be representative of equilibrium thermodynamic averages. Similar equilibration times were found in recent Car-Parrinello MD simulations using a Nose-Hoover thermostat [52]. In Fig.4.6, we show a snapshot of the simulated water structure.

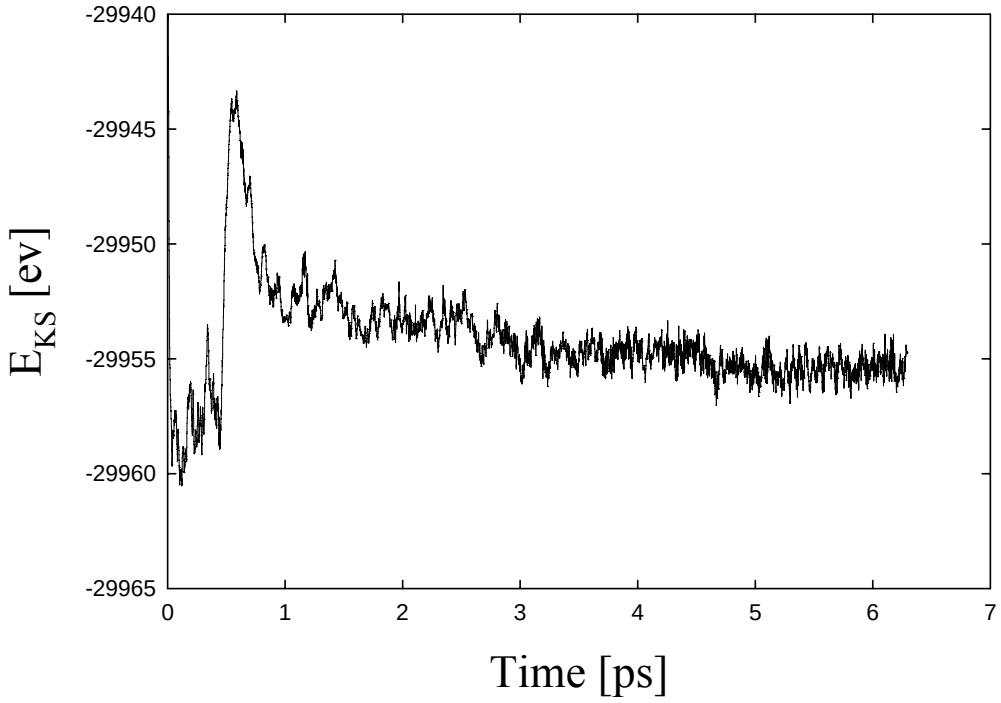

Figure 4.5: Time-dependence of the potential energy (i.e. Kohn-Sham energy) from an MD simulation of liquid water. The simulation shows little drift after the first 2.5 *ps* of equilibration time.

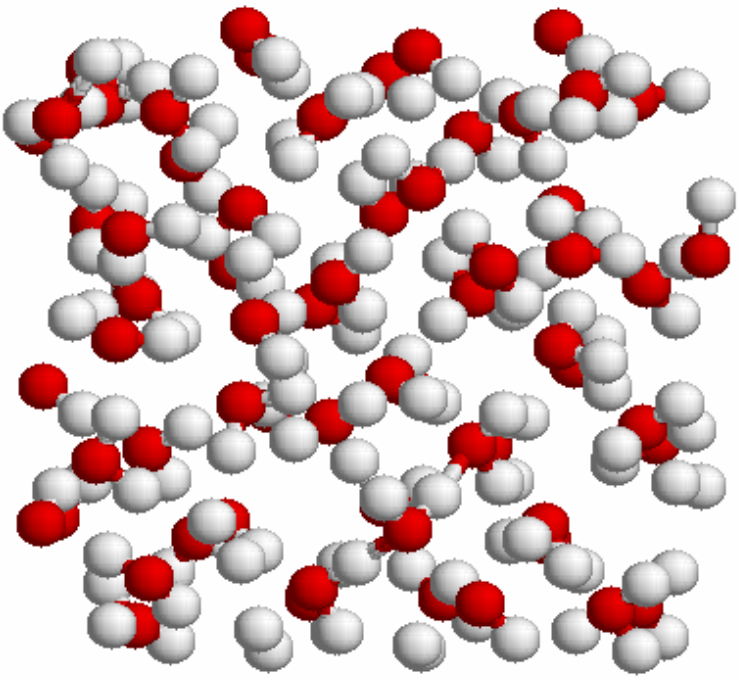

Figure 4.6: Snapshot of the structure of simulated water. The simulation cell contained 64 water molecules. The white spheres are hydrogen ions, and the dark spheres represent the oxygen ions.

After equilibration, we computed that time-averaged radial distribution functions for the remaining 4ps of simulation time. The results for H-H, O-H, and O-O pairs are shown in Fig. 4.7a-c with a comparison to experimental neutron scattering results [78]. We focus here on the case of ΔE_{PAO} = 8.0mRyd because, of the three basis sets explored in detail, it results in the best agreement with experiment. Comparable to other first-principles simulations, we find a significant overstructuring of the liquid, indicating that the hydrogen bonds are possibly too strong. For example, in Fig. 4.7c, the maximum height of the first peak at 2.75Å, $g_{OO}^{\max}$, is about

3.5 units, compared to about 2.8 units high in the experimental data. Similar differences can be seen comparing the simulated $g_{HH}(r)$ and $g_{OH}(r)$ to experiment. In addition to peaks that are too sharp and have too high amplitude, the structure in the liquid persists out to distances significantly longer than in experiment. Similar overstructuring, although not always as severe, has been observed in other first-principles calculations. For example, a recent paper reporting several different simulations using BLYP functionals but different system sizes and ensembles yields an average value of 3.0 for $g_{OO}^{\max}$. However, there is a wide range of values for $g_{OO}^{\max}$ reported from other first-principles simulations. For example, recent first-principles Car-Parrinello MD simulations using both the Perdew-Burke-Ernzerhoff (PBE) [79] and BLYP functionals results in a value of $g_{OO}^{\max} = 3.6$ [80, 81]. The results presented in Ref. [81] and Ref. [80] seem to also be in good agreement with another study by Asthagiri *et al*.[82] using PBE functionals but with the dynamics following the exact Born-Oppenheimer energy surface. One of the key results of Ref. [80] was that large values of the fictitious mass for the electronic degrees of freedom can lead to an unrealistic softening of the water interactions. In summary, there still remain questions about the ability of first-principles DFT to describe liquid water. As a result, it seems possible that the main limitations of our SIESTA model for water stem mostly from inherent errors in the GGA.

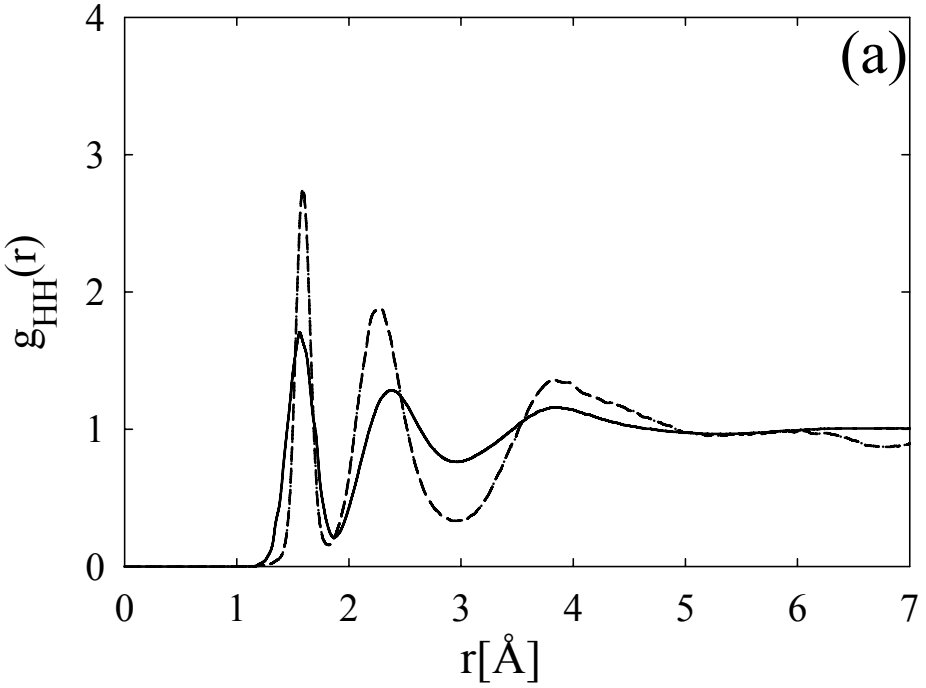
(a)
$g_{HH}(r)$
r[Å]
0
1
2
3
4
5
6
7

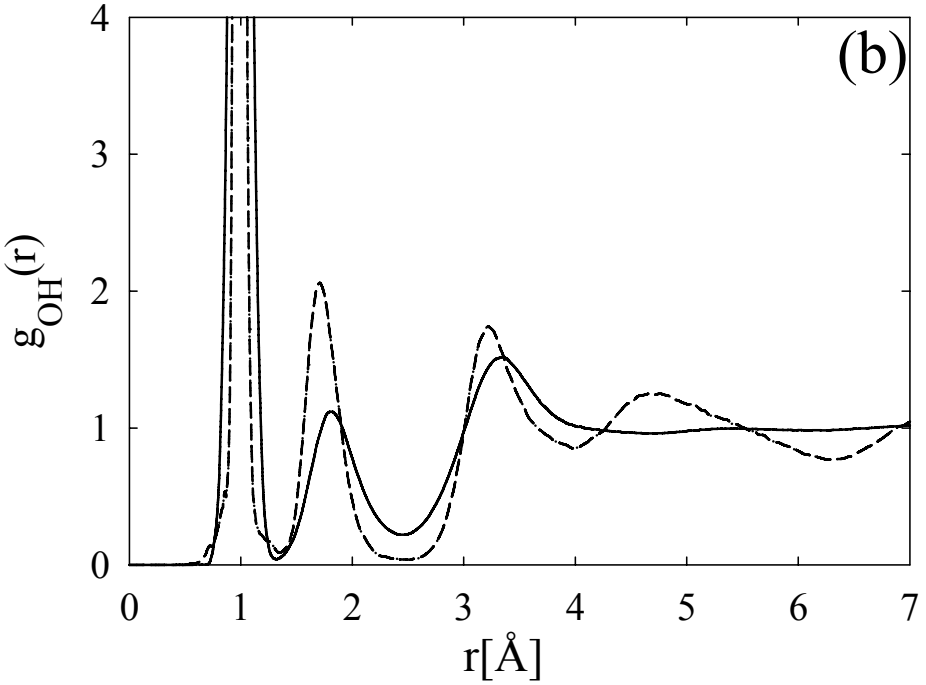
(b)
$g_{OH}(r)$
r[Å]
0
1
2
3
4
5
6
7

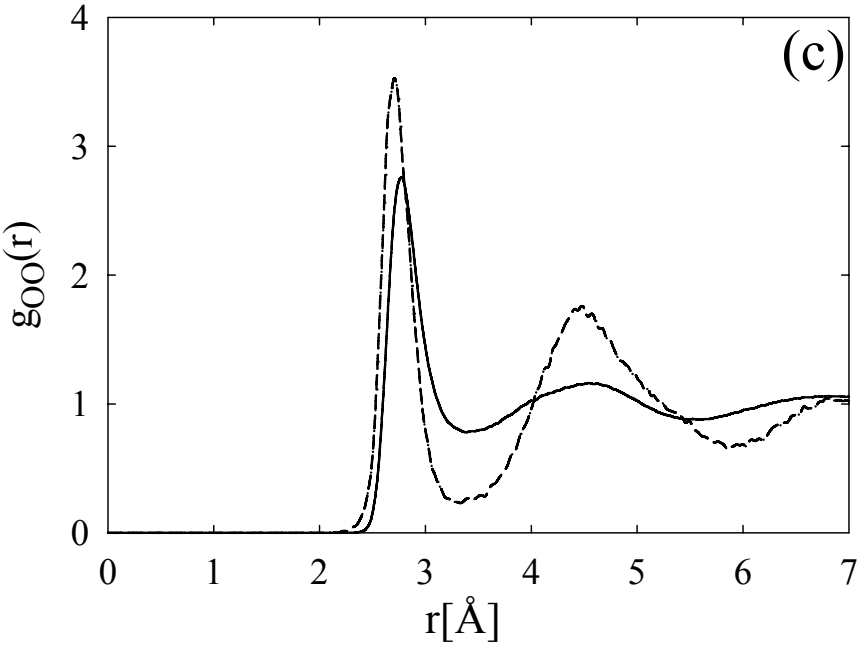

Figure 4.7: Radial distribution functions for (a) H-H, (b) O-H, and (c) O-O pairs from an MD simulation at T=315K (dashed line) using the PAO basis set corresponds to ΔE_{PAO}= 8.0*mRyd*. Also shown are the experimental results (solid line) from neutron scattering data [78]. In each case, the SIESTA MD simulations show significant overstructuring of the liquid.

In Fig. 4.8 we show a comparison between the three different PAO basis sets for $g_{OO}(r)$. The overstructuring of the liquid clearly is even more pronounced for the PAO basis sets corresponding to ΔE_{PAO}= 10.0mRyd and ΔE_{PAO}= 12.5mRyd. For example, $g_{OO}^{\max}$ increases from 3.5 to 4.5 as ΔE_{PAO} increases from 8.0mRyd to 12.5mRyd. Because increasing ΔE_{PAO} is directly connected to an increasing binding energy for the isolated water dimer, our results clearly show the overstructuring of the liquid can be directly linked to the strength of the hydrogen bonds. Surprisingly, however, the results of Fig. 4.2 indicate that each of the PAO basis states used to

generate the results of Fig. 4.8 in fact results in a dimer binding energy which is in fact smaller than experiment. However, as pointed out earlier, uncertainty in the experimental results is quite significant. On the other hand, the overstructuring of the liquid could be due to other factors. For example, it is possible that the results for the dimer are not entirely transferable to the liquid. Another possibility is that finite-size effects are significant. Finite-size effects have possibly been observed in other first-principles simulations of liquid water [52]. This issue is discussed more in the next section.

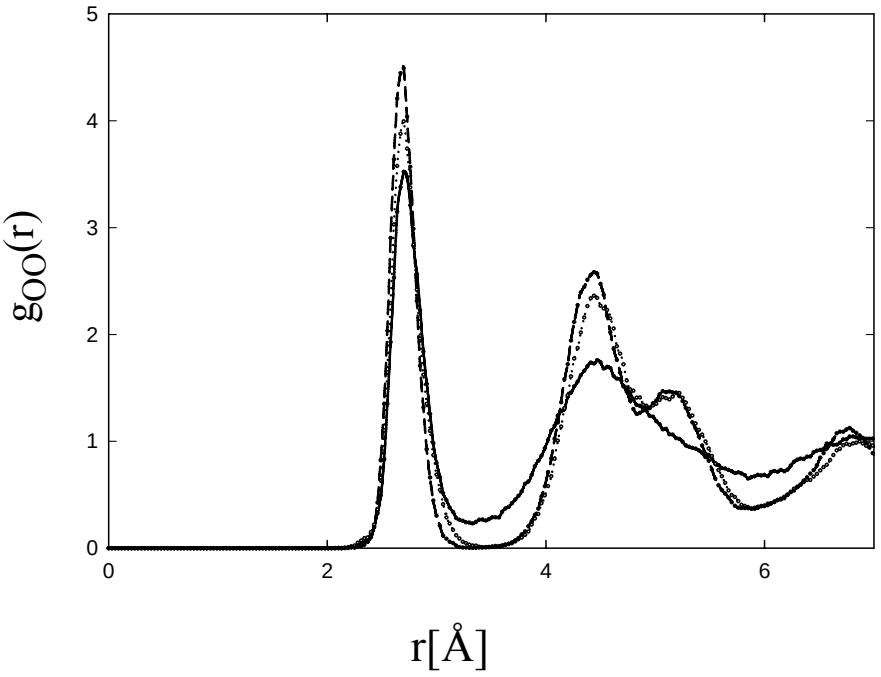

Figure 4.8: Comparison of the $g_{OO}(r)$ for three different basis sets corresponding to ΔE_{PAO} = 8.0*mRyd* (thick solid line), ΔE_{PAO} = 10.0 *mRyd* (dotted line), and ΔE_{PAO} = 12.5 *mRyd* (dashed line). The maximum in the first peak, $g_{OO}^{\max}$, increases systematically as the value of ΔE_{PAO} increases. This behavior is consistent with our observations that dimer binding energy is also increasing with values of ΔE_{PAO}. The best agreement with experiment occurs for ΔE_{PAO} = 8.0 *mRyd*.

Table 4.2: Self-diffusion coefficients computed using SIESTA. For comparison we include previous first-principles results and experimental values. Comparable to Car-Parinello MD (CPMD) simulations, SIESTA exhibits self-diffusion coefficients significantly below experimental measurements.

	Temperature [K]	D[$\mathring{A}^2/ps$]
SIESTA (this work)	315	0.006
CPMD [52, 80]	295-345	0.006-0.04
Expt [83]	315	0.35

Another important measure of the liquid is the self-diffusion coefficient for a water molecule. The self-diffusion coefficient was determined from the Einstein formula $6Dt = \left\langle \left| \vec{r}(t) - \vec{r}(0) \right|^2 \right\rangle$, where the angle brackets denote an average over time as well as each water molecule in the simulation. In Table 4.2 we show our results compared with experiment [83] and other first-principles calculations [52, 80]. In each case, the first-principles results significantly underestimate the self-diffusion coefficient. It may be, as others have suggested, that the time scales accessible to first-principles calculations are inadequate to study self-diffusion. However, a simple estimate indicates that using the Einstein formula and the experimental self-diffusion constant indicates that the average distance that a water molecule should diffuse in 10ps is on the order of 4Å, which is obviously significant enough to observe in our simulations and should be long enough for the Einstein relation to be valid. It seems more likely that the first-principles models are consistently predicting hydrogen bonds that are too

strong, and this error is responsible for the discrepancies between computed and experimental the radial distribution functions and self-diffusion coefficients.

In summary, the best PAO basis set with ΔE_{PAO} results in overstructured behavior when compared to experiment, but within the range of other first-principles results. The dimer binding energy and structure characterized by $g_{OO}^{\max}$ vary in a systematic manner with ΔE_{PAO}, suggesting a possible strategy to optimize the PAO basis set to further improve agreement with experiment. Comparable to prior first-principles results, the self-diffusion coefficient of water is greatly underestimated by simulation.

Discussion and Summary

We have identified a reasonable basis set for simulation of liquid water using the SIESTA electronic-structure code. The PAO basis corresponding to ΔE_{PAO} = 8.0mRyd provided the most reasonable model for water in comparison to experimental results for structure. However, the best model we obtained still exhibits overstructured behavior that manifests itself through peaks in the radial distribution functions that are higher than what is observed in experiment. This behavior has been seen previously in first-principles calculations, although in some instances to a somewhat lesser extent.

It is very likely that a better basis set can be identified for SIESTA. For example, Fig. 4.2 and Fig. 4.8 together suggest that by choosing a basis set with a weaker dimer binding energy, it should be possible to decrease the amount of short- and medium-range order and bring the peaks of the radial distribution functions into better agreement with experiment. While the dimer

binding energy for the PAO basis set with ΔE_{PAO} = 8.0mRyd provides a reasonable value for the dimer binding energy, ΔE_{PAO} of 6.0 mRyd might also provide a reasonable description of the dimer. However, because electronic-structure calculations more accurate than the SIESTA model used here show significant disagreement with experiment, it seems unjustified to attempt to improve the agreement of SIESTA beyond the accuracy of a traditional *ab initio* calculation. It seems more fruitful to attempt to improve the SIESTA model by improving agreement with more accurate ab initio results. In short, errors in SIESTA due to the finite basis set should be minimized in a sensible way, but fundamental errors in the GGA should not be compensated for by the choice of basis set.

A previous LCAO model due to Ortega *et al* [54] resulted in better agreement with experimental radial distribution functions than the results of our study. While many aspects of their approach are similar to SIESTA, there are some important differences. For the work in Ref. [54], the molecular orbitals of the water molecule were fixed and the Hamiltonian described only the weak intermolecular bonds (i.e. the hydrogen bonds). The internal coordinates of the water molecule were not allowed to change dynamically. As a result, the molecules in Ref. [54] were rigid and not polarizable. The argument in favor of this approach is that it permits a focus on the weak (~0.2eV) dimer binding energies. However, it is not clear what the effect of these restrictions is on the structure and dynamics. It seems very likely that dimer binding might be increased by allowing the water molecule to relax its internal degrees of freedom, both electronic and ionic. Entropic effects are also very different for rigid molecules compared to molecules with internal degrees of freedom. There are other differences between our work and the prior study that make direct comparison difficult. For example, the simulation here contained only 64 molecules, whereas the prior work contained 216 molecules. Another important difference is the

rather short simulation time of 2.0ps used in the prior study, compared to 6.5ps for the work described here. Based on the observations of other authors, it is possible that 2.0ps is too short a simulation time for full equilibration, and it cannot be ruled out that the computed radial distribution functions might evolve to something different for a longer simulation. In short, it is very hard to make a direct comparison of the merits of the SIESTA model and PAO basis we develop here and the prior LCAO simulations of Ref. [54].

It is interesting to speculate about the appropriate dimer binding energy for realistic first-principles simulation of liquid water. For example, the LDA approximation predicts a dimer binding energy that is far too strong [51]. As a result, LDA simulations of liquid water fail dramatically. The apparent tendency of the GGA is to underestimate the experimental dimer binding energy. For example, the dimer binding energy using the BLYP functional has been computed to be 4.3kcal/mol compared to the experimental value of 5.4kcal/mol [51]. For the MD simulations reported here, the basis set with a binding energy of 4.05kcal/mol results in the closest agreement to experiment. Interestingly, there is consensus that GGA simulations of liquid water tend to result in an overstructured liquid and diffusion constants that are perhaps two orders of magnitude below experiment. This behavior seems to be more consistent with a dimer binding energy which is too large rather than too small. Several possible factors could account for these issues. On the one hand, there is a significant amount of uncertainty in the experimental dimer binding energy. On the other hand, for MD simulations of liquid water, it is often difficult to compare different approaches. For example, recent first-principles simulations of water raised the possibility that Carr-Parrinello MD may result in different behavior when compared to Born-Oppenheimer dynamics for certain choices of the fictitious electronic mass [52, 80-82]. Furthermore, calculations within the microcanonical ensemble may lead to nonergodic behavior

especially in the vicinity of phase transitions. Finite-size effects might be a significant source of error, although there are some indications that while finite-size effects exist, they are relatively insignificant [80, 81].

Another effect that might be an important cause of disagreement between SIESTA and experiment is incomplete cancellation of errors due to the well-known basis-set superposition error [74]. This effect occurs often in LCAO-type approaches, and tends to result in models that are not transferable to different problems. It is due to the fact that the energy of a system tends to decrease as the size of the basis set increases. So, for example, while we expect that bonding between water molecules in a dimer should lower the energy, there is an additional spurious effect that results from an increase in the size of the basis which will improve (i.e. decrease) the energy of a water monomer. The basis-set superposition error should be different for liquid water and a water dimer, although it is unclear how important the effect might be. Therefore, while the dimer binding energy predicted by the $\Delta E_{PAO} = 8.0$mRyd basis is somewhat below experimental observations, it is possible that the interactions between water molecules in liquid water are still too strong due to basis-set superposition error. If this is the case, then it seems likely that, while the basis set might be tuned to achieve apparent good agreement with experiment, it may be necessary in fact to develop a new model with a larger PAO basis set so that basis-set superposition error is less significant. In other words, it may be the case that, without a larger basis, it is not possible to simultaneously predict accurately the dimer binding energy and structure of liquid water.

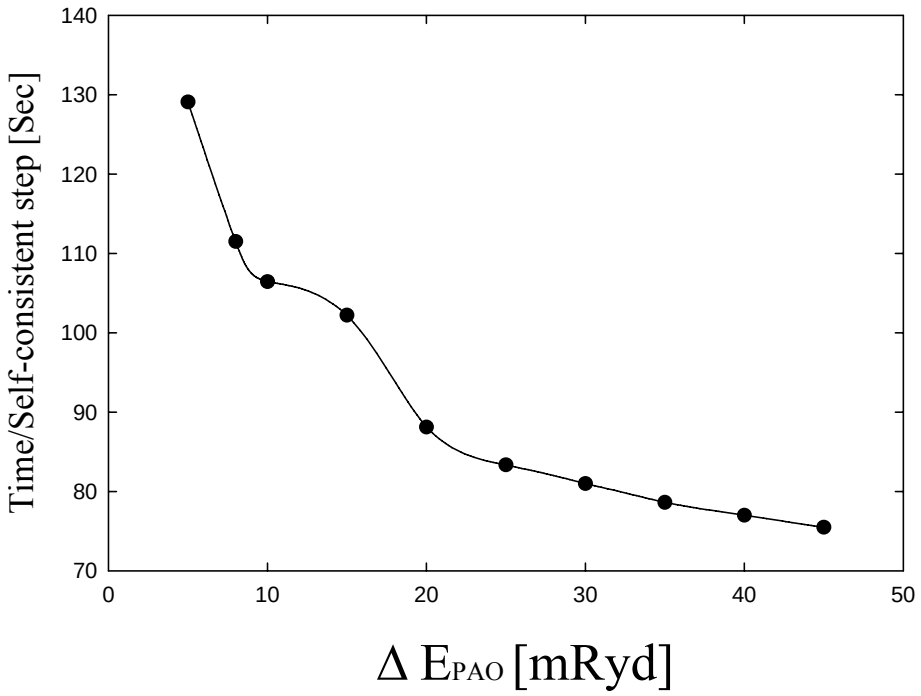

Figure 4.9: Computer time per self-consistent step as a function of ΔE_{PAO}. It is clear that the best basis sets for a realistic description of liquid water also result in the longest computation times. For the basis with $\Delta E_{PAO} = 8.0 mRyd$, each MD step takes about 20-25 minutes of real time on a single processor.

As with other first-principles approaches, the computational time associated with SIESTA remains a significant obstacle to applications. For the ΔE_{PAO} = 8.0mRyd basis, each self consistent step took about 105 seconds of processor time on a single 3.06GHz Pentium IV processor. A typical MD step required about 13-14 self-consistent steps to be adequately converged, resulting in a time of about 20-25 minutes for each MD step. While our results suggest that it might be possible to improve our results by choosing a PAO basis with a smaller value of ΔE_{PAO}, the results of Fig. 4.9 suggest that this may not be very practical. For example, for ΔE_{PAO} = 6.0mRyd, the computational time should increase by at least 10 seconds per step.

For ΔE_{PAO} = 4.0mRyd, the time increases to about 130 seconds for each self-consistent step. The dependence of the computational time on the PAO basis is directly linked to the degree of localization of the basis set. As ΔE_{PAO} decreases, the basis correspondingly becomes less localized. This increases that amount of computation required to determine the matrix elements of the single-particle Hamiltonian and overlap matrix. In addition, as the matrices become less sparse, the time for matrix diagonalization also increases. One approach to speed up the calculation that we did not pursue is to use the parallel version of the code. However, while this approach would decrease the real time needed for a calculation, it would not decrease the total computational load.

A much more promising approach is to use the O(N) algorithm already implemented in the SIESTA code. The approach that SIESTA uses is to create a truncated basis of Wannier functions [55-57]. While this is an approximate method that requires extensive testing to assure that the model is still reasonably accurate, it has been shown that the O(N) method in SIESTA will systematically converge to the exact result as the cutoff distance for the Wannier functions is increased. We have not tested this approach, but it is clearly the only alternative for large-scale simulation of ~10^3 or ~10^4 molecules. One obvious issue is that the wave functions for the water model are only periodic due to the unrealistic periodic nature of the simulation supercell. Therefore, it is not entirely clear how the O(N) method can be realistically applied to the study of liquid water. Another important question that must be answered is at what point (i.e. for how many molecules) the O(N) method becomes advantageous over direct diagonalization. If the crossover point is on the order of 100 molecules, application of the O(N) method might be quite useful for ~10^3 or even ~10^4molecule systems. On the other hand, if the crossover is nearer to

10^3 molecules, for example, the O(N) method is certain to be impractical, and the study of systems with 10^3 or more molecules is likely to remain out of reach for SIESTA.

In summary, we have found a reasonable PAO basis for simulation of liquid water using the SIESTA electronic-structure code and the BLYP energy functional. The best basis set we studied resulted in a liquid with more short- and medium-range structure than is observed in experiment. We found the liquid simulated by SIESTA to be overstructured to a degree at least comparable to traditional ab initio simulations using GGA functionals [52, 80-82]. By considering the systematic behavior of the liquid as the PAO basis set is varied, we have shown that it should indeed be possible to make further improvements in the model. However, it is not clear whether errors in the SIESTA model result from errors in the DFT or errors due to the finite PAO basis. In short, significant care must be exercised before LCAO methods such as SIESTA can be applied to problems involving liquid water. It seems likely that applications of SIESTA to large-scale simulation of problems involving liquid water will require use of the O(N) algorithm in SIESTA, although there remain many open questions about the feasibility of this approach.

CHAPTER 5 : GOLD OXIDE CLUSTER

Introduction

We have also studied the adsorption of oxygen molecule on gold clusters. Traditionally, gold has been known to be one of the least reactive metals in the bulk phase and hence has been regarded as relatively unimportant catalysts [84]. However, recent experiments have shown that, when dispersed as fine particles on metal oxide surfaces, gold facilitates a wide range of oxidation reactions, in particular the $CO \rightarrow CO_2$ oxidation [85-87]. The activity of gold clusters has been found to depend critically on the size of the particle and on the nature of the substrate [84]. Nanoparticles of gold supported on metal oxides have been shown to be very active for several reactions such as CO oxidation or low-temperature water gas shift (WGS) [88]. The catalysis of the WGS reaction over supported gold catalysts is a key step in applications such as on-board H_2 production via reforming processes for fuel cell applications. Apart from catalytic activities gold nanoclusters has also been used as nanoscale building block in materials and devices.

In this work we have studied the stability of neutral Au_n and Au_nO_2 (n=1-6) clusters and also tried to predict the activation energy and reaction path for the oxygen adsorption on the Au_6 cluster.

Computational Approach

The basic technical details of the calculation performed for this work is same as that of chapter 3. We used spin polarized density functional calculations with generalized gradient approximation of Wang and Perdew (PW91) using VASP program [89]. We used same parameter as used in work done by G. Mills *et al* [90] i.e. we used a plane wave basis set, with a kinetic energy cutoff of 396 *eV*. We used Monkhorst Gaussian smearing. We used PAW method for our studies where as G. Mills *el al* [90] used ultrasoft pseudopotentials. We only studied neutral gold clusters.

Results

We first calculated the binding energies of clusters of gold atoms Au_n with n varying from 1-6. From the earlier works it was clear that gold clusters with few atoms are stable only in a particular geometrical arrangements [90, 91]. In Fig. 5.1 we show the binding energy variation of our cluster of gold particles in comparison with earlier results [84]. We find that binding energies per atoms for our gold cluster increases continuously with cluster size. We have also calculated binding energies of a oxygen molecules to the gold cluster of different sizes and compared it with earlier results [90]. We computed the total energy of the system by computing forces and completely relaxing them. In Fig. 5.2 we show the binding energies of oxygen molecule to the gold cluster of different sizes. From the figure it is clear that we are in a good qualitative agreement with the previous DFT results. There is slight difference in the binding energies values from the previous results which is due to the fact that we have used PAW method where as Mills and coworkers [90] have used ultrasoft pseudopotentials implemented in VASP. The PAW approach is expected to be more accurate over plane-wave pseudopotential

methods because it uses a mixed basis of local orbitals and plane-waves and hence can account for core electrons in the appropriate local environment (e.g. in the cluster). As observed in the previous studies we also observed that molecular oxygen is more strongly bound to the neutral cluster with odd number of atoms as gold atoms have single electron in its outermost orbit *i.e.* 6*s* and they bind to oxygen molecule through charge transfer to the antibonding orbitals of O_2 [90].

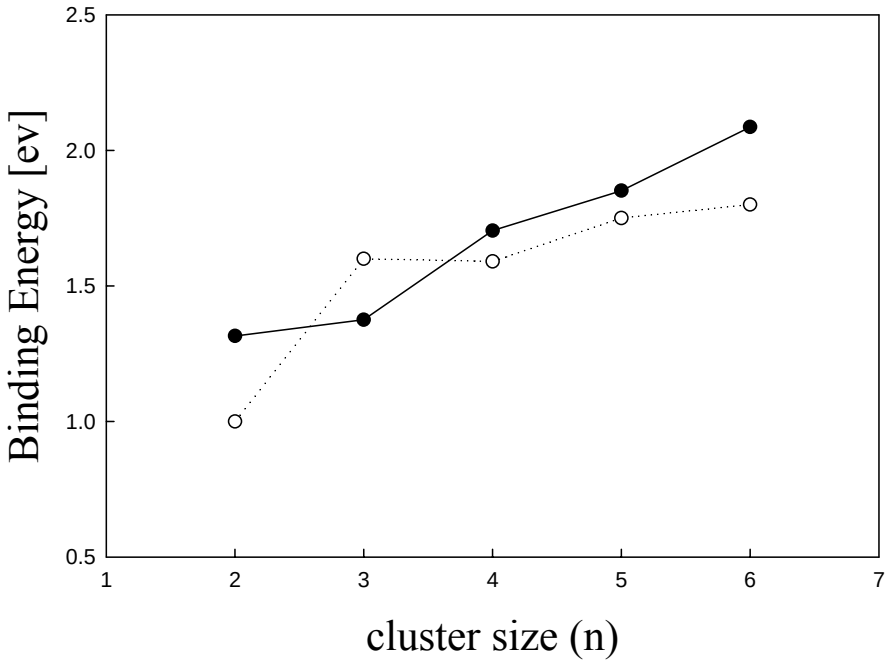

Figure 5.1: The plot shows the binding energies per atom of the gold cluster of different sizes in comparison with earlier DFT result. Solid line is the results from this work where as dotted line is results taken from ref. [84].

Binding energy of oxygen molecule to the gold cluster is calculated using following equation

$$E_b(O_2) = E(Au_n)+E(O_2)-E(Au_nO_2) \qquad 5.1$$

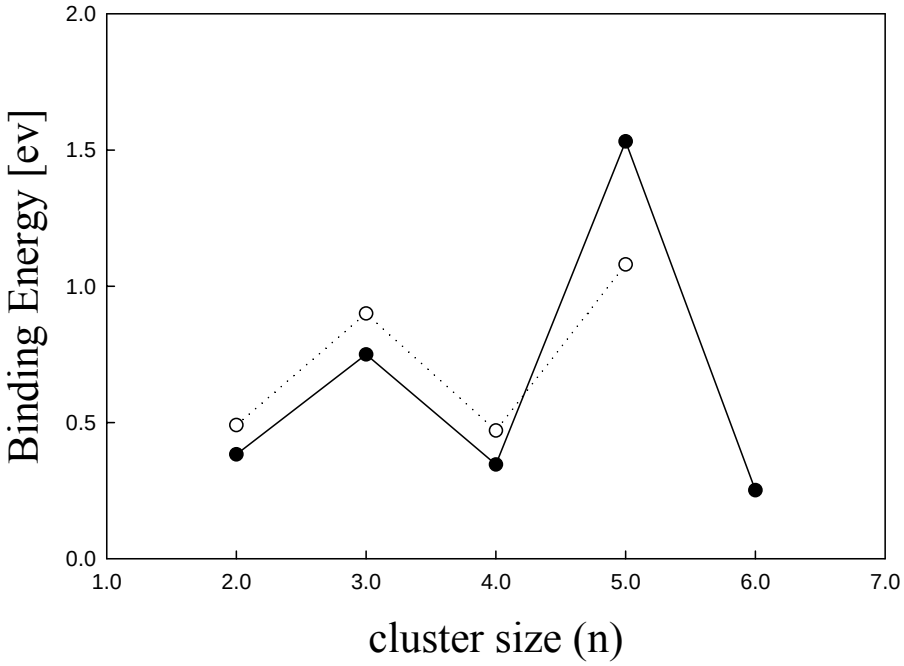

Figure 5.2: The plot shows the variation of binding energy of oxygen molecule to the gold cluster of different size. Solid line is the results from this work where as dotted line is from the ref. [90].

For any catalytic application we needed to investigate the dissociation of an oxygen molecule adsorbed on the gold cluster. This requires knowledge not only of the molecularly adsorbed state, but also of the dissociatively adsorbed final state. In general, we find that for larger clusters dissociative adsorption is energetically favorable, and there must be an activation barrier that characterizes the reaction. To explore the kinetics of the reaction (i.e. the activation barrier), we have chosen to study dissociation at the Au_6 cluster. We found that there are many metastable low energy states of oxygen atoms binding to the gold cluster. In Fig. 5.3 we show the lowest energy configuration of two oxygen atoms bound to Au_6 which is same as one shown by Yoon B. and his co-worker [92]. But we also found that there is more than one low energy metastable states for the oxygen molecule to bind to Au_6 cluster. In Fig. 5.4 we show a couple of low energy configurations of an oxygen molecule bound to Au_6.

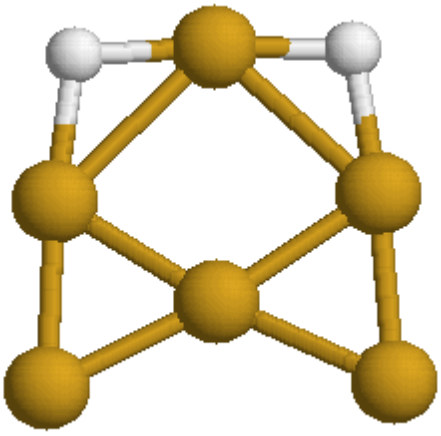

Figure 5.3: Ball-and-stick model of Au_6O_2 showing lowest energy configuration for Au_6O_2. Smaller spheres are oxygen atom and larger spheres are gold atoms. Here oxygen is attached atomically to the gold cluster. We find this is the ground—state structure for adsorbed oxygen.

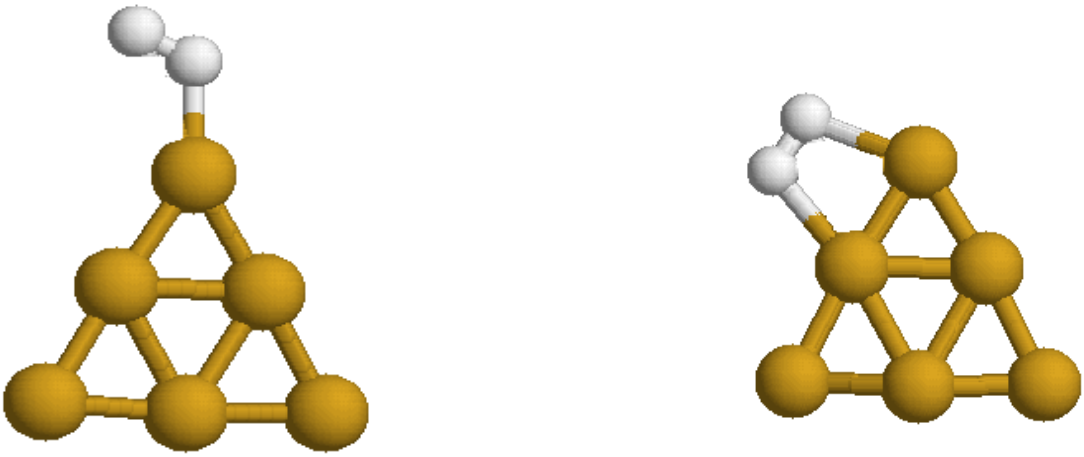

Figure 5.4: Ball-and-stick model of Au_6O_2 showing the metastable low energy configurations of Oxygen molecules bound to gold cluster. Smaller spheres are oxygen atom and larger spheres are gold atoms. Note that here oxygen is attached molecularly to the gold cluster.

Yoon B. and co-workers have shown a particular reaction pathway for the dissociation of O2 molecule for anion $Au_6O_2^-$ cluster using "nudged elastic band method". The nudged elastic band method is used to find Minimum Energy Path (MEP) when both the initial and final states are known [93]. In this method an elastic band, made of beads connected by harmonic springs, is strung between the reactant and product states. Using a set of images to define a discrete transition path, the problem is turned into a minimization problem by defining an object function [93].

$$F(\mathbf{r}_1, \mathbf{r}_2, ...\mathbf{r}_{p-1}) = \sum_{i=1}^{P-1} V(\mathbf{r}_i) + \sum_{i=1}^{P} \frac{kP}{2} (\mathbf{r}_i - \mathbf{r}_{i-1})^2 \qquad (5.2)$$

where the first sum is over the true potential of all the intermediate images of the system, and the second sum is "spring energy" that keeps the adjacent images together. The end point images $\mathbf{r}_o$ and $\mathbf{r}_p$ are fixed. In order to accelerate the convergence of the chain to the MEP we introduce "nudging". The component of the net spring force on a bead parallel to the local path tends to keep the bead equidistant from neighbors; whereas the perpendicular spring force tend to make it collinear with the neighbors. When the MEP is curved, the perpendicular spring force will tend to pull the chain off the MEP, thereby introducing the corner cutting thus making the perpendicular component of the spring force zero. Each image also feels a force due to the gradient of the "real" potential energy. The perpendicular component of this gradient force pulls the images down towards MEP and parallel component of this gradient force towards either reactant or product state, away from the saddle point. The problem of corner cutting and sliding down is cured by nudging *i.e* by projecting out the perpendicular component of spring force and the parallel component of true force. These force projections decouple the dynamics of the path itself from the particular distribution of images chosen in discreet representation of the path. The spring force then does not interfere with the relaxation of images perpendicular to the path and

the relaxed configuration of the images satisfies $\nabla V(\mathbf{r}_i)|_{\perp} = 0$. Which in other words they lie on MEP [93-95].

Using this nudged elastic band method, Yoon *et al* calculated activation barrier for dissociation at [92] anionic $Au_6O_2^-$ clusters to be 2.33 *eV*. They have calculated the activation energy for neutral Au_6O_2 and cationic $Au_6O_2^+$ clusters as well and were found to be well above 3 *eV* which implies that this reaction pathway is very unlikely due to very slow kinetics of the reaction. However, the work of Yoon et al. [92] considered only the left panel of Fig. 5.4 as the initial state and Fig. 5.3 as the initial state. Because there are other metastable states, however, it may be that there is some other intermediate state which will then involve two barriers for the reaction that may be lower than the barrier found by Yoon et al. We are considering the structure shown in the right panel of Fig. 5.4 as an intermediate state. Our preliminary results suggest that this indeed may result in a lower activation barrier. We found that there is difference of 0.72 *eV* in the binding energy of intermediate state i.e. structure in the right panel of Fig 5.4 and the structure shown in Fig. 5.3 which suggests there may be a lower activation barrier for the dissociation of oxygen molecule from the gold cluster. While our initial results are enticing, a more careful analysis using the nudged elastic band method is underway.

Discussion and future work

To understand any catalytic reaction it is very important to know about minimum energy paths for any reaction. Although, we got few low energy geometrical configurations for Au_6O_2 which suggest there is possibility of existence of reaction pathway with activation barrier much below 3.0 *eV* but nothing can be said with certainty unless we get results from much proven

"nudged elastic band" method for our system. We have been able to implement nudged elastic band method for our system and currently we are looking for the reaction barrier and low energy path. To fully understand the catalytic behavior of gold cluster we also need to study it on some kind of oxide substrate to relate it with possible experimental studies. As it has been found that choice of oxide support affect the activity of gold nanoparticles [96]. For example, gold cluster supported at the reducible oxides like TiO_2 and Fe_2O_3 yield larger CO_2 production than nonreducible oxides like MgO and SiO_2 [97-99]. This study usually proves quite difficult due to the intensive nature of VASP calculations. Future studies that can access experimental time and length scales might involve less expensive approaches, possibly SIESTA or some other limited basis-set method, including tight-binding [7, 27-29].

LIST OF REFERENCES

1. Trovarelli, A., et al., *The utilization of ceria in industrial catalysis.* Catalysis Today, 1999. **50**(2): p. 353-367.
2. Lahaye, J., et al., *Influence of cerium oxide on the formation and oxidation of soot.* Combustion and Flame, 1996. **104**(1-2): p. 199-207.
3. Matatov-Meytal, Y.I. and M. Sheintuch, *Catalytic abatement of water pollutants.* Industrial & Engineering Chemistry Research, 1998. **37**(2): p. 309-326.
4. Liu, W. and M. Flytzanistephanopoulos, *Total Oxidation of Carbon-Monoxide and Methane over Transition Metal-Fluorite Oxide Composite Catalysts .2. Catalyst Characterization and Reaction-Kinetics.* Journal of Catalysis, 1995. **153**(2): p. 317-332.
5. Campbell, C.T. and C.H.F. Peden, *Oxygen Vacancies and Catalysis on Ceria Surfaces.* Science, 2005. **309**(5735): p. 713.
6. Lindan, P.J.D., N.M. Harrison, and M.J. Gillan, *Mixed dissociative and molecular adsorption of water on the rutile (110) surface.* Physical Review Letters, 1998. **80**(4): p. 762-765.
7. Schelling, P.K., N. Yu, and J.W. Halley, *Self-consistent tight-binding atomic-relaxation model of titanium dioxide.* Physical Review B, 1998. **58**(3): p. 1279-1293.
8. Kundakovic, L., D.R. Mullins, and S.H. Overbury, *Adsorption and reaction of H2O and CO on oxidized and reduced Rh/CeOx(111) surfaces.* Surface Science, 2000. **457**(1-2): p. 51-62.

9. Otsuka, K., M. Hatano, and A. Morikawa, *Hydrogen from Water by Reduced Cerium Oxide.* Journal of Catalysis, 1983. **79**(2): p. 493-496.

10. Padeste, C., N.W. Cant, and D.L. Trimm, *The Influence of Water on the Reduction and Reoxidation of Ceria.* Catalysis Letters, 1993. **18**(3): p. 305-316.

11. Berner, U., et al., *Ultrathin ordered CeO2 overlayers on Pt(111): interaction with NO2, NO, H2O and CO.* Surface Science, 2000. **467**(1-3): p. 201-213.

12. Henderson, M.A., et al., *Redox properties of water on the oxidized and reduced surfaces of CeO2(111).* Surface Science, 2003. **526**(1-2): p. 1-18.

13. Marder, M.P., *Condensed Matter Physics* Third ed. 2000: A Wiley-Interscience Publication, New York.

14. Parr, R.G. and W. Yang, *Density-Functional Theory of Atoms and Molecules* 1989: Oxford University Press. 51-52.

15. Payne, M.C., et al., *Iterative Minimization Techniques for Abinitio Total-Energy Calculations - Molecular-Dynamics and Conjugate Gradients.* Reviews of Modern Physics, 1992. **64**(4): p. 1045-1097.

16. Ihm, J., A. Zunger, and M.L. Cohen, *Momentum-Space Formalism for the Total Energy of Solids.* Journal of Physics C-Solid State Physics, 1979. **12**(21): p. 4409-4422.

17. Kresse, G. and J. Furthmuller, *Efficient iterative schemes for ab initio total-energy calculations using a plane-wave basis set.* Physical Review B, 1996. **54**(16): p. 11169-11186.

18. Kresse, G. and J. Furthmuller, *Efficiency of ab-initio total energy calculations for metals and semiconductors using a plane-wave basis set.* Computational Materials Science, 1996. **6**(1): p. 15-50.

19. Kresse, G. and J. Hafner, *Ab-Initio Molecular-Dynamics Simulation of the Liquid-Metal Amorphous-Semiconductor Transition in Germanium.* Physical Review B, 1994. **49**(20): p. 14251-14269.

20. Kresse, G. and J. Hafner, *Norm-Conserving and Ultrasoft Pseudopotentials for First-Row and Transition-Elements.* Journal of Physics-Condensed Matter, 1994. **6**(40): p. 8245-8257.

21. Laasonen, K., et al., *Car-Parrinello Molecular-Dynamics with Vanderbilt Ultrasoft Pseudopotentials.* Physical Review B, 1993. **47**(16): p. 10142-10153.

22. Pasquarello, A., et al., *Abinitio Molecular-Dynamics for D-Electron Systems - Liquid Copper at 1500-K.* Physical Review Letters, 1992. **69**(13): p. 1982-1985.

23. Vanderbilt, D., *Soft Self-Consistent Pseudopotentials in a Generalized Eigenvalue Formalism.* Physical Review B, 1990. **41**(11): p. 7892-7895.

24. N. W. Ashcroft and N.D. Mermin, *Solid state physics* 1976: Holt Rinehart and Winston, New York,.

25. Johnson, D.D., *Modified Broyden Method for Accelerating Convergence in Self-Consistent Calculations.* Physical Review B, 1988. **38**(18): p. 12807-12813.

26. Pulay, P., *Convergence Acceleration of Iterative Sequences - the Case of Scf Iteration.* Chemical Physics Letters, 1980. **73**(2): p. 393-398.

27. Menon, M. and K.R. Subbaswamy, *Nonorthogonal tight-binding molecular-dynamics study of silicon clusters.* Physical Review B, 1993. **47**(19): p. 12754.

28. Porezag, D., et al., *Construction of tight-binding-like potentials on the basis of density-functional theory: Application to carbon.* Physical Review B, 1995. **51**(19): p. 12947.

29. Tang, M.S., et al., *Environment-dependent tight-binding potential model.* Physical Review B, 1996. **53**(3): p. 979.

30. Pickard, C.J. and B.r. Winkler, *Structural Properties of Lanthanide and Actinide Compounds within the Plane Wave Pseudopotential Approach.* Physical Review Letters, 2000. **85**(24): p. 5122.

31. Skorodumova, N.V., et al., *Quantum origin of the oxygen storage capability of ceria.* Physical Review Letters, 2002. **89**(16): p. 166601.

32. Yang, Z.X., et al., *Atomic and electronic structure of unreduced and reduced CeO2 surfaces: A first-principles study.* Journal of Chemical Physics, 2004. **120**(16): p. 7741-7749.

33. Blochl, P.E., *Projector Augmented-Wave Method.* Physical Review B, 1994. **50**(24): p. 17953-17979.

34. Perdew, J.P., et al., *Atoms, Molecules, Solids, and Surfaces - Applications of the Generalized Gradient Approximation for Exchange and Correlation.* Physical Review B, 1992. **46**(11): p. 6671-6687.

35. Gerward, L., POWDER DIFFR 1993. **8**: p. 127.

36. Nakajima, A., A. Yoshihara, and M. Ishigame, *Defect-Induced Raman-Spectra in Doped Ceo2.* Physical Review B, 1994. **50**(18): p. 13297-13307.

37. Monkhorst, H.J. and J.D. Pack, *Special points for Brillouin-zone integrations.* Physical Review B, 1976. **13**(12): p. 5188.

38. Baudin, M., M. Wojcik, and K. Hermansson, *Dynamics, structure and energetics of the (111), (011) and (001) surfaces of ceria.* Surface Science, 2000. **468**(1-3): p. 51-61.

39. Conesa, J.C., *Computer Modeling of Surfaces and Defects on Cerium Dioxide.* Surface Science, 1995. **339**(3): p. 337-352.

40. Esch, F., et al., *Electron localization determines defect formation on ceria substrates.* Science, 2005. **309**(5735): p. 752-755.

41. Norenberg, H. and G.A.D. Briggs, *Defect structure of nonstoichiometric CeO2(111) surfaces studied by scanning tunneling microscopy.* Physical Review Letters, 1997. **79**(21): p. 4222-4225.

42. Van Bavel, A.P., D. Curulla Ferre, and J.W. Niemantsverdriet, *Simulating temperature programmed desorption directly from density functional calculations: How adsorbate configurations relate to desorption features.* Chemical Physics Letters, 2005. **407**(1-3): p. 227-231.

43. Redhead, P.A., *Thermal desorption of gases.* Vacuum, 1962. **12**(4): p. 203-211.

44. Skorodumova, N.V., M. Baudin, and K. Hermansson, *Surface properties of CeO2 from first principles.* Physical Review B, 2004. **69**(7).

45. Halley, J.W., J.R. Rustad, and A. Rahman, *A Polarizable, Dissociating Molecular-Dynamics Model for Liquid Water.* Journal of Chemical Physics, 1993. **98**(5): p. 4110-4119.

46. Sprik, M. and M.L. Klein, *A Polarizable Model for Water Using Distributed Charge Sites.* Journal of Chemical Physics, 1988. **89**(12): p. 7556-7560.

47. Stilling.Fh and A. Rahman, *Improved Simulation of Liquid Water by Molecular-Dynamics.* Journal of Chemical Physics, 1974. **60**(4): p. 1545-1557.

48. Toukan, K. and A. Rahman, *Molecular-Dynamics Study of Atomic Motions in Water.* Physical Review B, 1985. **31**(5): p. 2643-2648.

49. Dang, L.X., *The Nonadditive Intermolecular Potential for Water Revised.* Journal of Chemical Physics, 1992. **97**(4): p. 2659-2660.

50. Laasonen, K., F. Csajka, and M. Parrinello, *Water Dimer Properties in the Gradient-Corrected Density Functional Theory.* Chemical Physics Letters, 1992. **194**(3): p. 172-174.

51. Sprik, M., J. Hutter, and M. Parrinello, *Ab initio molecular dynamics simulation of liquid water: Comparison three gradient-corrected density functionals.* Journal of Chemical Physics, 1996. **105**(3): p. 1142-1152.

52. Kuo, I.F.W., et al., *Liquid water from first principles: Investigation of different sampling approaches.* Journal of Physical Chemistry B, 2004. **108**(34): p. 12990-12998.

53. Laasonen, K., et al., *Ab-Initio Liquid Water.* Journal of Chemical Physics, 1993. **99**(11): p. 9080-9089.

54. Ortega, J., J.P. Lewis, and O.F. Sankey, *First principles simulations of fluid water: The radial distribution functions.* Journal of Chemical Physics, 1997. **106**(9): p. 3696-3702.

55. Ordejon, P., E. Artacho, and J.M. Soler, *Self-consistent order-N density-functional calculations for very large systems.* Physical Review B, 1996. **53**(16): p. 10441-10444.

56. Ordejon, P., et al., *Linear System-Size Scaling Methods for Electronic-Structure Calculations.* Physical Review B, 1995. **51**(3): p. 1456-1476.

57. Soler, J.M., et al., *The SIESTA method for ab initio order-N materials simulation.* Journal of Physics-Condensed Matter, 2002. **14**(11): p. 2745-2779.

58. Fernandez, E.M., R. Eglitis, and L.C.B. G. Borstel, *Adsorption and dissociation of water on relaxed alumina clusters: a first principles study.* physica status solidi (b), 2005. **242**(4): p. 807-809.

59. Hubsch, A., et al., *Optical conductivity of wet DNA.* Physical Review Letters, 2005. **94**(17).

60. Junquera, J., et al., *Numerical atomic orbitals for linear-scaling calculations.* Physical Review B, 2001. **64**(23).

61. Sankey, O.F. and D.J. Niklewski, *Abinitio Multicenter Tight-Binding Model for Molecular-Dynamics Simulations and Other Applications in Covalent Systems.* Physical Review B, 1989. **40**(6): p. 3979-3995.

62. Artacho, E., et al., *Linear-scaling ab-initio calculations for large and complex systems.* Physica Status Solidi B-Basic Research, 1999. **215**(1): p. 809-817.

63. Becke, A.D., *Density-functional exchange-energy approximation with correct asymptotic behavior.* Phys. Rev. A, 1988. **38**(6): p. 3098.

64. Lee, C.T., W.T. Yang, and R.G. Parr, *Development of the Colle-Salvetti Correlation-Energy Formula into a Functional of the Electron-Density.* Physical Review B, 1988. **37**(2): p. 785-789.

65. Troullier, N. and J.L. Martins, *Efficient Pseudopotentials for Plane-Wave Calculations.* Physical Review B, 1991. **43**(3): p. 1993-2006.

66. Kleinman, L. and D.M. Bylander, *Efficacious Form for Model Pseudopotentials.* Physical Review Letters, 1982. **48**(20): p. 1425-1428.

67. Curtiss, L.A., D.J. Frurip, and M. Blander, *Studies of Molecular Association in H2o and D2o Vapors by Measurement of Thermal-Conductivity.* Journal of Chemical Physics, 1979. **71**(6): p. 2703-2711.

68. Reimers, J.R., R.O. Watts, and M.L. Klein, *Intermolecular Potential Functions and the Properties of Water.* Chemical Physics, 1982. **64**(1): p. 95-114.

69. Odutola, J.A. and T.R. Dyke, *Partially Deuterated Water Dimers - Microwave-Spectra and Structure.* Journal of Chemical Physics, 1980. **72**(9): p. 5062-5070.

70. Tursi, A. and E. Nixon, J. Chem. Phys, 1970. **52**: p. 1521.

71. Kuchitsu, K. and Y. Morino, *Estimation of Anharmonic Potential Constants .2. Bent Xy2 Molecules.* Bulletin of the Chemical Society of Japan, 1965. **38**(5): p. 814-&.

72. Benedict, W.S. and N.a.E.K.P. Gailan, Journal of Chemical Physics, 1956. **24**: p. 1139.

73. Clough, S.A., et al., *Dipole-Moment of Water from Stark Measurements of H2o, Hdo, and D2o.* Journal of Chemical Physics, 1973. **59**(5): p. 2254-2259.

74. Szalewicz, K., et al., *A Theoretical-Study of the Water Dimer Interaction.* Journal of Chemical Physics, 1988. **89**(6): p. 3662-3673.

75. Hoover, W.G., *Canonical Dynamics - Equilibrium Phase-Space Distributions.* Physical Review A, 1985. **31**(3): p. 1695-1697.

76. Nose, S., *A Molecular-Dynamics Method for Simulations in the Canonical Ensemble.* Molecular Physics, 1984. **52**(2): p. 255-268.

77. Parrinello, M. and A. Rahman, *Crystal-Structure and Pair Potentials - a Molecular-Dynamics Study.* Physical Review Letters, 1980. **45**(14): p. 1196-1199.

78. Soper, A.K., *The radial distribution functions of water and ice from 220 to 673 K and at pressures up to 400 MPa.* Chemical Physics, 2000. **258**(2-3): p. 121-137.

79. Perdew, J.P., K. Burke, and M. Ernzerhof, *Generalized gradient approximation made simple.* Physical Review Letters, 1996. **77**(18): p. 3865-3868.

80. Grossman, J.C., et al., *Towards an assessment of the accuracy of density functional theory for first principles simulations of water.* Journal of Chemical Physics, 2004. **120**(1): p. 300-311.

81. Schwegler, E., et al., *Towards an assessment of the accuracy of density functional theory for first principles simulations of water. II.* Journal of Chemical Physics, 2004. **121**(11): p. 5400-5409.

82. Ashthagiri, D., L. Pratt, and K. J., Phys. Rev. E., 2003. **68**: p. 041505.

83. Mills, R.J., J. Phys. Chem, 1973. **77**: p. 685.

84. Wu, X., et al., *A density functional study of carbon monoxide adsorption on small cationic, neutral, and anionic gold clusters.* Journal of Chemical Physics, 2002. **117**(8): p. 4010-4015.

85. Grunwaldt, J.D. and A. Baiker, *Gold/titania interfaces and their role in carbon monoxide oxidation.* Journal of Physical Chemistry B, 1999. **103**(6): p. 1002-1012.

86. Haruta, M., *Size- and support-dependency in the catalysis of gold.* Catalysis Today, 1997. **36**(1): p. 153-166.

87. Valden, M., X. Lai, and D.W. Goodman, *Onset of catalytic activity of gold clusters on titania with the appearance of nonmetallic properties.* Science, 1998. **281**(5383): p. 1647-1650.

88. Fu, Q., H. Saltsburg, and M. Flytzani-Stephanopoulos, *Active nonmetallic Au and Pt species on ceria-based water-gas shift catalysts.* Science, 2003. **301**(5635): p. 935-938.

89. Wang, Y. and J.P. Perdew, *Correlation hole of the spin-polarized electron gas, with exact small-wave-vector and high-density scaling.* Physical Review B, 1991. **44**(24): p. 13298.

90. Mills, G., M.S. Gordon, and H. Metiu, *The adsorption of molecular oxygen on neutral and negative Au-n clusters (n=2-5).* Chemical Physics Letters, 2002. **359**(5-6): p. 493-499.

91. Soule de Bas, B., M.J. Ford, and M.B. Cortie, *Low energy strucutre of gold nanoclusters in the size range 3-38 atoms.* Journal of Molecular Structure (Theochem), 2004. **686**: p. 193.

92. Yoon, B., H. Hakkinen, and U. Landman, *Interaction of O-2 with gold clusters: Molecular and dissociative adsorption.* Journal of Physical Chemistry A, 2003. **107**(20): p. 4066-4071.

93. Mills, G., H. Jonsson, and G.K. Schenter, *Reversible Work Transition-State Theory - Application to Dissociative Adsorption of Hydrogen.* Surface Science, 1995. **324**(2-3): p. 305-337.

94. Jonsson, H., G. Mills, and K.W. Jacobsen, *Nudged Elastic Band Method for Finding Minimum Energy Paths of Transitions*, in *Classical and Quantum Dynamics in Condensed Phase Simulations*. 1998, World Scientific.

95. Schenter, G.K., G. Mills, and H. Jonsson, *Reversible Work Based Quantum Transition-State Theory.* Journal of Chemical Physics, 1994. **101**(10): p. 8964-8971.

96. Wolf, A. and F. Schuth, *A systematic study of the synthesis conditions for the preparation of highly active gold catalysts.* Applied Catalysis a-General, 2002. **226**(1-2): p. 1-13.

97. Gluhoi, A.C., M.A.P. Dekkers, and B.E. Nieuwenhuys, *Comparative studies of the N2O/H-2, N2O/CO, H-2/O-2 and CO/O-2 reactions on supported gold catalysts: effect of the addition of various oxides.* Journal of Catalysis, 2003. **219**(1): p. 197-205.

98. Grisel, R.J.H. and B.E. Nieuwenhuys, *Selective oxidation of CO over supported Au catalysts.* Journal of Catalysis, 2001. **199**(1): p. 48-59.

99. Schubert, M.M., et al., *CO oxidation over supported gold catalysts-"inert" and "active" support materials and their role for the oxygen supply during reaction.* Journal of Catalysis, 2001. **197**(1): p. 113-122.